

Development of a Diffusion Mobility Database for Co-based Superalloys

Greta Lindwall¹, Kil-won Moon², Maureen Williams² Whitney Tso³ Carelyn Campbell²

¹Royal Institute of Technology (KTH), Department of Material Science and Engineering, Brinellvägen 23, SE-100 44 Stockholm, Sweden

²National Institute of Standards and Technology, Materials Science and Engineering Division, Gaithersburg, MD 20899

³Northwestern University, Department of Materials Science and Engineering, Evanston, IL 60208

Abstract

To facilitate the development of high-temperature Co-based γ - γ' superalloys, a Co-Ni based diffusion mobility database is developed for the eight component FCC (Face Centered Cubic) system of Co-Al-W-Ni-Cr-Ti-Ta-Re. A CALPHAD approach is used to represent the temperature and composition dependency of the multicomponent system. The mobility descriptions are based on previous assessment work for the Ni-based superalloys, published experimental and computational data, and established diffusion correlations. The initial mobility descriptions were then refined using additional diffusion couple experimental data, particularly for the Co-Cr, Co-Ta, and Ni-Ta systems. After re-optimizing the descriptions with the new experimental data, the mobility descriptions were validated using a collection of published diffusion couple composition profiles, which were not included in the initial assessment process.

I. Introduction

Since the report by Sato et al. [1] of a two-phase γ - γ' microstructure present in Co-Al-W alloys, work has accelerated to develop high temperature Co-based superalloys that could replace current γ - γ' Ni-base superalloys, such as Inconel 718, and increase the operating temperatures of aerospace turbine engines and land-based industrial gas turbines [2]. This alloy development effort has motivated the development of a variety of CALPHAD-based thermodynamic and diffusion mobility descriptions to facilitate the design of these new alloys. Essential for these designs is the ability to predict the microstructure stability of these new alloys during extended service times at high temperatures, particularly the creep resistance. One technique to enhance the creep resistance is dependent on reducing the diffusivity in the FCC (Face-Centered Cubic, γ) matrix phase. Lass [3] used a CALPHAD-based approach to design an improved Co-Ni γ '-strengthened alloy using available commercial and published thermodynamic databases. Other recent design efforts include the work by Ruan et al. [4] to develop W-free, high-strength Co superalloys using machine learning and CALPHAD. Liu et al. [5] employed machine learning techniques to optimize a γ ' strengthened Co-base superalloy.

For many of the recent γ - γ' Co-based superalloy designs it is of particular interest to consider more effective use of the alloying additions to improve the creep resistance of the material by

slowing the coarsening of the γ - γ' microstructure. First-principles calculations [6] have suggested that a large solute-vacancy binding energy would reduce the mobilities of the solute and the vacancy, thus increase the stability of the microstructure. Naghavi et al. [6] calculated the solute-vacancy binding energies for all the transition metal elements in FCC Co matrix. A parabolic trend was observed as a function of the d -occupancy across the transition metal element with smaller binding energies predicted at the center of the series. In addition, it was noted that larger solute atoms had stronger binding energies as result of the larger strains associated with the larger atoms. Density functional theory (DFT) calculations by Neumeier et al. [7] predicted that the bonding electron charge density increased along the $\langle 110 \rangle$ direction between Re and nearby Co atoms, suggesting that there is an additional contribution to increase solute-vacancy binding energy associated with Re in FCC-Co.

To design a novel high temperature Co superalloys, suitable for both traditional solidification casting processing and additive manufacturing power bed fusion methods, the Center for Hierarchical Materials Design (CHiMaD) [8] is working towards the development of a set of self-consistent CALPHAD-based thermodynamic and diffusion mobility databases. The thermodynamic database is based on previous work to develop a Ni-based superalloy database [9]. The current thermodynamic description includes four solution phases (liquid, FCC (γ), BCC (Body Center Cubic), and HCP (hexagonal close-packed)), three ordered phases (B2, $L1_2(\gamma')$, $D0_{19}$), six topological close-packed (TCP) phases (μ , σ , C14, C15, C36, $D0_{22}$), and over 50 intermetallic phases [10-12] [13, 14]. While the descriptions for the TCP phases continue to be developed, the description of the FCC phase is well-established and is available at materialsdata.nist.gov.

This work presents the current mobility descriptions for the Co FCC (γ) phase in the Co-Al-W-Ni-Cr-Ti-Ta-Re system. The NIST nickel-based diffusion mobility database [15] [16] was used as the foundation for the developing these new Co-Ni-based diffusion mobility descriptions. The initial Ni-based diffusion mobility database emphasized assessment of the Ni-based binary diffusion mobility descriptions. The current work is focused on the assessment of the Co-based binary diffusion mobility descriptions and *maintaining* compatibility with current Ni-based assessments. Additional experimental binary and ternary diffusion couples are evaluated at two different temperatures and used to improve the assessments. The resulting new database is suitable for both Co and Ni-base alloys.

II. Background

a. CALPHAD-approach

A CALPHAD-approach for describing the composition and temperature dependent diffusion mobilities in a given phase has been well-established [17] [18] and applied to variety of systems [15] [19]. The approach is briefly reviewed here. When a vacancy exchange mechanism in a crystalline phase is assumed, the diffusion coefficient in the lattice-fixed frame of reference, D_{kj}^L , is defined as function of the atomic mobility and the thermodynamic factor as follows:

$$D_{kj}^L = \sum_{i=1}^n M_{ki}^L \frac{\partial \mu_i}{\partial x_j} \quad (1)$$

where j is the diffusing species, k is the gradient species and M is the atomic mobility. The thermodynamic factor is the partial derivative of the chemical potential, μ , with respect to the mole fraction x_j of the diffusing species. If the molar volumes are assumed to be constant, the diffusivities can be transformed to the volume-fixed frame of reference by the following equation:

$$D_{kj}^V = \sum_{i=1}^n (\delta_{ik} - x_k) x_i M_i \frac{\partial \mu_i}{\partial x_j} \quad (2)$$

where δ_{ki} is the Kronecker delta symbol and is equal to one when $i = k$, and zero when $i \neq k$. M_i is the mobility of species i in a given phase.

The M_{ki}^L matrix, which is both composition and temperature dependent, defines the diffusion mobility in the lattice-fixed frame of reference. In the lattice-fixed frame of reference, the correlation effects are assumed to be negligible, and the off-diagonal terms of the mobility matrix are zero. Thus, the diagonal terms of the mobility matrix are:

$$M_{ki}^L = \delta_{ki} x_i M_i$$

$$M_i = \Theta_i \frac{1}{RT} \exp\left(\frac{\Delta Q_i^*}{RT}\right) \quad (3)$$

Θ_i represents the effects of the atomic jump distance (squared) and the jump frequency and has the units of m^2/s . ΔQ_i^* is the diffusion activation energy of species i in a given phase with units of (J/mol).

$$\Delta Q_i^* = \sum_j x_j Q_i^j + \sum_p \sum_{j>p} x_p x_j \sum_k {}^k A_i^{pj} (x_p - x_j)^k \quad (4)$$

where the Q_i^j and the ${}^k A_i^{pj}$ are linear functions of temperature.

The CALPHAD approach to model multicomponent systems is based on combining unary, binary, and ternary phase-based composition and temperature descriptions to extrapolate to n -components. The assumption is that in metallic systems, true quaternary and higher order phases are rare. Based on this, the CALPHAD-approach for developing diffusion mobilities relies on the availability of thermodynamic descriptions for the multicomponent multi-phase system of interest, computational and experimental data to describe the mobilities in the phases of interest, and the diffusion correlations to estimate mobility values for non-stable end-members (e.g. the self-diffusion of W in pure FCC W). First-principles approaches are used to predict the impurity diffusivities and activation energies. Experimental tracer diffusivity data, interdiffusion coefficients, obtained from measured composition profiles, and multiple diffusion

couple composition profiles are essential for optimizing and validating the diffusion mobility descriptions.

b. First-Principles Calculations

Naghavi et al. [20] used first-principles theory to predict the diffusivities of the transition metals in FCC Co assuming that the primary diffusion mechanism is vacancy driven nearest-neighbor hops that could be modeled using a five-frequency model. The Perdew-Burke-Ernzerhof (PBE) approximations were determined to yield the most accurate activation energies when compared to experimental results for the self-diffusion of FCC Co. Phonon calculations were included to explicitly allow for the determination of the effective jump frequency and vacancy migration entropy, which are required to estimate the effective diffusivities (D_0). The calculations indicated that the activation energies and solute-diffusivities follow a parabolic trend across the transition metal series, with the slowest diffusivities and highest activation energies predicted for the elements near the middle of the series.

c. Diffusion Correlations

Diffusion correlations are used in the assessment process when experimental data and first-principles calculations are not available. This is particularly important for defining unstable end-members required by the CALPHAD method (e.g. the self-diffusion of W in FCC-W or the diffusivity of Co in FCC-Ta). Diffusion correlations may also be used when the experimental data are sparse and an initial estimate is needed. For the self-diffusion coefficients, several correlations between the activation energy and the melting temperature [21] or the crystal structure have been developed [22],[23], [24]. Based on the analysis of the data in 30 different binary systems, Xin et al. [25] proposed a new empirical relationship between the self-diffusion and the impurity diffusion in FCC binary solutions where the product of the self-diffusivities is equal to the product of the impurity diffusivities, which makes it possible to predict one diffusivity in a binary system where the other three are known:

$$D_i^i D_j^j = D_i^j D_j^i \quad (5)$$

where D_i^i is the self-diffusion of element i in the FCC matrix of i and D_j^i is the impurity diffusivity of element i in the FCC matrix of j .

III. Summary of previous work

Recently there have been several experimental studies and CALPHAD assessments of the diffusion Co-based systems, which are summarized in Table 1. In addition, a similar effort to improve the multicomponent diffusion mobility descriptions for Ni-based superalloys containing Co was recently published by Liu et. al [19]. That work focused on the Ni-rich Ni-Al-Ti-Cr-Co-Mo-Ta-W system considering additional experimental data from a diffusion multiple with Ni and three multicomponent alloys at 1300 °C.

Table 1. Experimental and assessed diffusion mobilities of the Co-based system

System	Annealing Temperature (°C)	Reference	Notes
Co-Al	469 - 639	[26]	Co diffusion in Al
Co-Al	359 - 629	[27]	Co diffusion in Al
Co-Cr	1000 - 1300	[28]	Cr diffusion in Co
Co-Cr	1000 - 1360	[29]	Diffusion coefficients
Co-Cr	1100, 1200, 1300	[7]	Activation energies, D_0 , interdiffusion coefficients
Co-Ni	1050 - 1250	[30]	Inter, impurity, intrinsic diffusion coefficients, activation energies
Co-Ni	600 - 1600	[31]	Assessment
Co-Ni	701-1297	[32]	Diffusion coefficients, activation energies
Co-Re	1100, 1200, 1300	[7]	Activation energies, D_0 , interdiffusion coefficients,
Co-Re	1000 - 1400	[33]	Assessment
Co-Ta	1100, 1200, 1300	[7]	Activation energies, D_0 , interdiffusion coefficients,
Co-Ti	1100, 1200, 1300	[7]	Activation energies, D_0 , interdiffusion coefficients
Co-Ti	700-1140	[34]	Co-Ti diffusion coefficients
Co-W	1000-1300	[35]	Inter and intrinsic diffusion coefficients; assessment
Co-W	1407- 1997	[36]	Co tracer diffusivity in W
Ni-Re	900-1400	[37]	Assessment
Ni-Re	900 - 1300	[38]	Interdiffusion coefficients
Ni-Re	1200, 1300	[39]	Interdiffusion coefficients
Ni-Ta	900-1400	[37]	Assessment
Ni-Ta	900 - 1300	[38]	Interdiffusion coefficients
Ni-Ti	1000 - 1300	[40]	Assessment
Ni-W	900-1400	[37]	Assessment
Ni-W	900 - 1300	[38]	Interdiffusion coefficients
Co-Al-Cr	1100, 1200	[41]	Interdiffusion coefficients
Co-Al-Ni	900 - 1300	[42]	Interdiffusion coefficients; assessment
Co-Al-Ni	800, 900	[43]	Isothermal section; composition profile
Co-Al-Ta	800, 900	[43]	Isothermal section; composition profile
Co-Al-Ti	1100, 1200	[44]	Diffusion couple profiles; assessment
Co-Al-W	900,	[43]	Isothermal section; composition profile
Co-Al-W	900, 1000	[45]	diffusion coefficients; assessment
Co-Al-W	900-1300	[46]	Diffusion multiples; assessment
Co-Cr-Ni	1150, 1200, 1250	[47]	Interdiffusion coefficients
Co-Cr-Ni	1150- 1250	[48]	Diffusion couples; assessment
Co-Cr-Ni	1300	[49]	Diffusion couples; assessment
Co-Cr-Ti	1050	[50]	Interdiffusion coefficients; assessment
Co-Cr-W	1100	[51]	Diffusion couple profiles; assessment
Cr-Ni-Ti	850 – 1000	[52]	Diffusion couple profiles; assessment
Co-Ni-Re	1050 - 1250	[53]	Interdiffusion coefficients; diffusion couple profiles
Co-Ni-Re	900 - 1400	[54]	Assessment

Co-Ni-W	1200, 1300	[55]	Interdiffusion coefficients; diffusion couple profiles
Co-Al-Cr-Ni	1150	[56]	Binary, ternary, and quaternary interdiffusion experiments
Co-Cr-Ni-Ti	1100	[57]	Interdiffusion experiments
Ni-Al-Ti-Cr-Co-Mo-Ta-W	1300	[19]	
Solutes in FCC Co	1100, 1200, 1300	[7]	Binary diffusion couples and first-principles Monte Carlo
Transition metal in FCC Co		[20]	Transition metals in FCC Co -DFT
Ni-Al-Ti-Cr-Co-Mo-Ta-W	1280	[58]	HitDIC Software

In addition to experimental and assessed data for diffusion in the FCC phase, data is available for the diffusion in Co-rich liquid phase. Walbrühl et al. [59] used *ab initio* molecular dynamics (AIMD) simulations to obtain diffusion data for Co self-diffusion and diffusion of a number of elements in liquid Co, including Ta, Ti and W. Their AIMD results were benchmarked against available literature data, including liquid Co self-diffusion, and used to simulate the diffusion in the liquid Co binder during gradient sintering of cemented carbides.

IV. Experimental and Computational Methods

a. Experimental Methods and Data Analysis

Based on the available experimental data and previous mobility assessments additional experimental diffusion couples were designed and measured to improve the mobility assessments for the multicomponent systems, particularly the Co-Cr-Ta and Ni-Cr-Ta systems. The end-member alloys were arc-melted from Co, Cr, Ni, and Ta elements, with purities in mass fraction of 99.9%, 99.99%, 99.9%, and 99.95%, respectively. The homogenization conditions and measured compositions of the end-members are summarized in Table 2. Some details of the end-members for Co-Al-W systems have been summarized in previous work [45].

Table 2: Summary of diffusion couple end-members and homogenization conditions.

	Nominal Composition (mole fraction)	Composition Analysis after Homogenization (mole fraction)				Homogenization Conditions
		Co	Cr	Ni	Ta	
<i>a</i>	Co	1.000				1320 °C for 6 h & 1250 °C for 60 h
<i>b</i>	Ni			1.000		
<i>c</i>	Co - 0.25Cr	0.745	0.255			1300 °C for 6 h & 1200 °C for 240 h
<i>d</i>	Ni - 0.01Ta			0.986	0.014	
<i>e</i>	Ni - 0.27Cr	0.726	0.274			1250 °C for 6 h & 1150 °C for 240 h
<i>f</i>	Ni - 0.09Ta			0.913	0.087	

The homogenized ingots were cut into pieces approximately 9 mm x 9 mm x 4.5 mm. All the pieces were ground and polished on both sides and finished with 1 μm diamond suspension. A diffusion couple stack with 21 interfaces was assembled to provide data for six binary diffusion couples and 14 ternary diffusion couples. A schematic of the stack is shown in Figure 1. All binary alloys used in the diffusion couple were single FCC compositions* and those compositions are given in Table 2. Note that the results for diffusion couple with Co-Al and Ni-Al alloys from this stack are not reported.

The prepared diffusion couple stacks were annealed at 900 °C, 1000 °C, and 1200 °C for 1300 h, 260 h, and 160 h, respectively. After the diffusion annealing, the stacks were mounted in epoxy, sectioned parallel to the columnar direction, ground and polished.

Data Smoothing

All the diffusion couples were examined using scanning electron microscopy (SEM) to ensure the quality of the bond regions. The grain size was noted to be larger than 250 μm so that grain boundary diffusion could be neglected. Composition profiles were measured using a JEOL JSM-7100 FE-SEM with an Oxford Instruments X-Maxn 80 silicon drift detector[†] with a 15 keV accelerating voltage and 0.7 nA probe current. The composition analysis was performed using the elemental standards, which were collected using a 1000 s acquisition time and using the Co K, Ni K, Cr L, Ta L, W L, and Al K lines. An initial composition profile measurement was performed to estimate overall penetration profiles. Based on the initial estimate of the diffusion penetration, each diffusion couple was measured using the point analysis mode across the diffusion zone using a 400 s acquisition time for each point. The diffusion zone included at least 40 points and increased up to 60 points according to the complexity of the diffusion profile. For each diffusion couple, four to seven parallel composition profiles were measured. All the experimental data are available at materialsdata.nist.gov.

Due to the composition variation in some of the profiles, particularly in the W and Ta end-member compositions, data smoothing is required, as well as defining the end-member compositions for each composition profile. For each composition versus distance data set, a discrete Fourier Gauss Filter with a 1 μm fill width half maximum (FWHM) filter was used to reduce the noise in the data. This process has been described previously by Moon et al. [45]. The end-member compositions for each diffusion couple data set are determined by averaging the measured compositions at each end of profile for a suitable distance (this is approximately the average of the last ten composition points at each end of the diffusion couple). After reducing the noise, a Fourier series function is used to fit the data in the diffusion zone by truncating the function where it intersects the constant end-member compositions for the diffusion couple. This composition function, representing a specific composition versus distance data set, is then fitted to a spline function.

* Note all compositions are given in mole fraction unless otherwise stated.

[†] Commercial names for instruments and software are used for completeness and do not constitute an endorsement from NIST.

An average Matano interface position must be determined to compare the current measured experimental data to the diffusion simulations predictions for a given diffusion couple. For a given diffusion couple, the Matano interface position is computed for each spline fitted data set. Then using the calculated averaged Matano interface position, the x -distance is corrected so that the Matano interface position is at zero. Using the averaged Matano plane as a reference, the shifted experimental data sets (for the given parallel line scans) are merged into a single data set, which is referred to as the **merged data**. The data smoothing process is then reapplied to the merged data set and a single spline function is fitted to the data, which is then used to compare with the calculated composition profiles using the CALPHAD-based mobility and thermodynamic descriptions. The interdiffusion coefficients were extracted from some of the binary diffusion couples using the Sauer-Freise method and using the method described previously by Moon et al [45].

b. Assessment Process

The current assessment of the FCC diffusion mobilities in the Co-Al-Cr-Ni-Ti-Ta-Re-W system was an iterative process. The first step was to use the previous NIST-Ni Mobility database [15] as a starting reference, then integrate both the Co-Al-Ni-W diffusion mobility assessment by Moon et. al. [45] and the first-principles predictions for the transition metal solute diffusivity predictions by Naghavi et al. [20]. The diffusion correlations by Askill [21] and Xin et al. [25] were then used to determine any missing end-member parameters. After this initial integration, the mobility database was evaluated using available literature data and experimental data to determine which binary and ternary systems require additional optimization.

The development of any CALPHAD-based multicomponent database requires a variety of compromises to achieve the optimal description. These compromises include: the weighting of various experimental and computational data sets from different sources, the optimization of the parameters that best fit the binary system versus improving the optimization within ternary systems, and the determination of how many higher order parameters should be included. In addition to these considerations, previous assessments should be considered particularly when evaluating the self-diffusion parameters for the pure components in different phases (i.e., the self-diffusion of Ni in FCC-Ni). While there is no established reference set of diffusion mobility parameters for the pure elements, as defined for the Gibbs free energy, there are some well-established mobility assessments for many of the pure elements that should be considered. Establishing and continuing the use of these reference parameters is essential for the further development of multicomponent databases. However, the use of these established mobility parameters for the pure components may limit the ability to obtain the best optimization for a given system. This work considers both optimization approaches. Initially, the self-diffusion mobility parameters are allowed to vary to enable the best possible fit to all the available data. The values for the established reference self-diffusivities are then included and followed by verification of the optimization to ensure that the quality of the initial fits from the full optimization are maintained.

For the diffusion mobilities in the liquid phase, the values calculated by AIMD [59] were directly added to the database. The diffusion of Re in FCC Co is not available and hence, it is assumed to be the same value as the diffusivity of W in FCC Co predicted by AIMD.

Simulation of Composition Profiles.

Composition profiles for binary and multicomponent diffusion couples are simulated using the finite-difference code, DICTRA [60, 61], and the current thermodynamics and diffusion mobility descriptions. The simulations assume that the end-member compositions are either the reported compositions or the average of the last five compositions at the end of each profile. All the simulations assume an initial sharp interface described by Heaviside functions. A double geometric grid was used for all the simulations. The macros for all the simulations are available at materialsdata.nist.gov

Optimization Methods

There are a variety of different tools available for optimizing CALPHAD-mobility parameters with respect to the measured composition profiles, including HitDIC [62], PyMob, [63], and the optimizer within DICTRA [64]. Two different methods were employed to optimize the individual mobility parameters for this work. For the experimental composition profiles collected as a part of this work, a MatLab code was coupled with the DICTRA diffusion simulation software to optimize the individual mobility parameters of interest by directly evaluating the difference between the measured composition profile for a given diffusion couple and the predicted composition profile.

For a given system, the specified mobility parameters are optimized using a simulated annealing method. The method generates a new point randomly based on a probability distribution that accepts only points that reduce the response error and avoids points that are trapped in local minima. The optimization space for the mobility parameters is initially defined by the previously published parameters. The simulated diffusion profiles are compared to the merged spline-fitted data as a function of temperature, and the square residuals are integrated as a sum of square error, based on Eq. 6:

$$\text{Err}(i) = \frac{1}{x_i^+ - x_i^-} \int_{x_i^-}^{x_i^+} \left\{ \frac{C_{x_i}^{\text{DICTRA}} - C_{x_i}^{\text{Merged}}}{C_i^{+\infty} - C_i^{-\infty}} \right\}^2 dx \quad (6)$$

where, Err(i) is a sum of the normalized square error of component i ; x_i^+ is x -distance to the right of the diffusion boundary; x_i^- is x -distance to the left of the diffusion boundary; $C_i^{+\infty}$ is the right end-member composition; $C_i^{-\infty}$ is the left end-member composition; $C_{x_i}^{\text{DICTRA}}$ is the composition of the DICTRA simulation at x -distance; and $C_{x_i}^{\text{Merged}}$ is the composition of merged spline-fitted data. The sum of the square error in Eq (6) is normalized by the diffusion distance and differences in the end-member compositions. The optimization algorithm is set to reduce this normalized square error by varying the mobility parameters.

For the Co-Ni-Re diffusion couples reported in the literature, a TC-Python code [65], similar to that described by Salmasi et al. [66], was implemented to also directly evaluate the mobilities from the composition profiles. The optimization using the TC-Python code included the simulation of the diffusion couple composition profiles using a specified set of mobility parameters and comparing these predictions to the measured profiles. The specified diffusion mobility parameters were optimized to minimize the difference between the measured and predicted composition profiles. To improve the accuracy the compositions near the interface were weighted twice as high as those composition approaching the end-member compositions.

V. Assessment Results and Validation

a. Self-diffusion in the stable FCC elements

The self-diffusion for the stable FCC elements, Ni and Al, were held constant based on the previous analysis by Campbell and Ruhkin [67]. While the stable crystal structure for Co is HCP at room temperature, FCC is the stable structure for Co above 422 °C. Cui et al. [68] evaluated the self-diffusion FCC-Co based on the available tracer diffusivity measurements and inputs from binary Co-Fe and Co-Ni diffusion couples. The temperature dependence of this assessment was modified slightly by Moon et al. [45] based on additional experimental data from binary Co-Al and Co-W diffusion couples. The comparison of the modified Co self-diffusivity with the previous assessment by Cui et al. [31] and the available tracer diffusivity data [69-72] is shown in Figure 2.

The remaining elements in the system (Cr, Ta, Ti, Re, and W) are not stable in the FCC phase; thus, experimental measurements of the self-diffusivity for these elements is not possible and a variety of different methods have been used to estimate the self-diffusivity. The self-diffusion of Cr was estimated by Jonsson [73] based on the predicted metastable FCC melting temperature (using the SGTE 1991 lattice stabilities [74]) and the diffusion correlations by Brown and Ashby [23] and Askill [21]. However, significant discrepancies have been associated with the Cr lattice stability [75], which could produce significant errors in the prediction of the metastable FCC melting temperature. Consequently, the Cr self-diffusivity in FCC-Cr is not well established. Similarly, the estimated self-diffusion parameters for Ti, Ta, Re, and W are based on the predicted FCC melting temperature and the diffusion correlations from Brown and Ashby [23].

Table 3. Summary of the self-diffusivities for the pure elements in the FCC phase

Element	Stable Crystal Structure	Mobility Parameter	Reference
Ni	FCC	-287000-69.8*T	[73]
Al	FCC	-126719-95.09*T	[76]
Co	HCP/FCC	-301795-72.25*T	This work
		-301,654-70.11*T	[31]
Cr	BCC	-235000-82*T;	[73]
Ta	BCC	-267428-78.51*T	This work
Ti	HCP	-261183-75.82*T	[15]

Re	HCP	-457520-71.88*T	[37]
W	BCC	-310679-67.73*T	This work

b. Updated binary assessments

Co-Cr

The diffusivity in the FCC phase of the binary Co-Cr system has been studied and assessed previously. The mobility parameters for the metastable FCC Cr were first evaluated by Jonsson [73]. Gómez-Acebo et al. [57], Zhang et al. [51] and Chen et al. [77] have also assessed the diffusion mobilities in the Co-Cr FCC system using the FCC-Cr self-diffusion mobility evaluated by Jonsson [73]. Zhang et al. [51] investigated the diffusivities in the Co-Cr-W system but only considered the additional experimental work done at 1100 °C. Chen et al. [77] evaluated the binary mobility interactions in the Ni-Al-Co-Cr system using the mobility end-members established by Gómez-Acebo et al. [57]. Neumeier et al. [7] also evaluated the diffusivity in the FCC Co-Cr system with both binary diffusion couples and first-principles calculations. These previous results were combined with the additional data from the Co/Co-0.25 Cr diffusion couple to optimize the binary interaction parameters and the diffusivity of Cr in FCC-Co and Co in FCC-Cr. Based on this optimization of the binary mobilities, the predicted composition profiles are compared to the measured profiles for the diffusion couple at 1200 °C in Figure 3. Table 4 (*see end of document for Table*) lists the optimized values for the system based on Eq 4 and the corresponding mobility database file is available at [materialsdata.nist.gov \(https://hdl.handle.net/11256/998\)](https://hdl.handle.net/11256/998). Figure 4 shows the comparison of the predicted interdiffusion coefficients as a function of the Cr composition using the current assessment (including the present and previous experimental work). The current assessment is in good agreement with the current measured diffusion coefficients at 1000 °C and at 1200 °C, and with the previously measured diffusion coefficients by Neumeier et al. [7] at 1100 °C, 1200 °C and 1300 °C. It is also noted that diffusion coefficients measured as a part this work at 1200 °C are in agreement with those measured by Neumeier et al. The current assessment predictions are also in relatively good agreement with the diffusion coefficient measured by Minamino et al. at 1150 °C [56]. The diffusion coefficients measured by Weeton [29] are not in agreement with current assessment; however, the measured coefficients are also three times greater than those measured by Neumeier et al. at 1300 °C. Due to the discrepancies with other reported experimental data the Weeton data are not considered in the assessment or validation process and are only plotted in Figure 4 as a reference.

Co-Ta

As a limited number of diffusivity experiments are available for the FCC Co-Ta system additional diffusion couples were evaluated at 1000 °C and 1200 °C. These data along with the experimentally determined interdiffusion coefficients at 1100 °C, 1200 °C and 1300 °C are included in the current optimization of the FCC Co-Ta system, which includes the following parameters Q_{Co}^{Ta} , Q_{Ta}^{Co} , Q_{Ta}^{Co} , ${}^0A_{Co}^{Co,Ta}$, and ${}^0A_{Ta}^{Co,Ta}$ (Table 4). Figure 5 shows a comparison of the experimental and predicted Ta composition profile for Co/Co-0.014 Ta diffusion couple at 1200 °C. This comparison shows good agreement between the measured and predicted Ta

compositions. Comparisons with the measured interdiffusion coefficients by Neumeier et al. [7] are in good agreement, as shown in Figure 6. The current optimization predicts an activation energy for Ta in FCC Co of 273.3 kJ/mol, which is within the estimated experimental activation energy $282.5 \text{ kJ/mol} \pm 6.0 \text{ kJ/mol}$ and the first-principles prediction 257.7 kJ/mol reported by Neumeier et al.

Ni-Ta

There is also limited experimental data for the diffusivity for Ta in FCC-Ni. Interdiffusion coefficients were measured by Karunaratne et al. [38] in the temperature range from 900 °C to 1300 °C. Additional binary Ni/Ni-0.087 Ta diffusion couples were analyzed to improve the multicomponent descriptions. Based on the two diffusion couples at 1000 °C and 1200 °C, the binary interaction parameters (${}^0A_{Ni}^{Ni,Ta}$ and ${}^0A_{Ta}^{Ni,Ta}$) and the Ta diffusivity in Ni (Q_{Ni}^{Ta}) and Ni diffusivity in Ta (Q_{Ta}^{Ni}) parameters were re-optimized. The current description for the mobilities in the Ni-Ta FCC phase is given in Table 4. The predicted and experimental composition profiles are shown in Figure 7 and the comparison with previous interdiffusion coefficient data is shown in Figure 8.

Co-Ti

The diffusivity of Ti in FCC-Co is assessed assuming that the diffusivity of Ti in FCC-Co is similar to that in FCC-Ni and using the previous assessment of the FCC-Ti self-diffusivity based, which is based on the binary and ternary diffusion couple measurements in the Ni-Ti [78] and [79] and Ni-Al-Ti [80] systems. More recently, others have re-evaluated the FCC Ti self-diffusivity based on the Askill correlation [21] using the metastable melting temperature of the FCC-Ti [50] [81] and additional Ni-Ti diffusion couple experiments [40]. The currently used activation energy (Q_{Ti}^{Ti}) assessed at (261.2 kJ/mol) is in relatively good agreement with the first-principles predictions from [20] (258 kJ/mol) and the experimental measurements by Neumeier et al. [7] (262.0 ± 8.2 kJ/mol). In contrast, the estimated activations in the assessments by Zhou and Liu (143.6 kJ/mol) [50] and Zhang et al. [82] (143.5 kJ/mol) are much lower than first-principles predictions and the experimental measurements. The diffusivities in Co-Ti system are optimized based on the interdiffusion coefficients measured by Neumeier et al. [7]. Figure 9 shows the comparison between the predicted and measured interdiffusion coefficients.

Ternary diffusion couples

Co-Ni-Ta and Co-Cr-Ta

The Co-Ni-Ta and Co-Cr-Ta ternaries are assessed using the Ni-Ta, Co-Ta and Co-Cr binaries and the previously assessed Co-Ni binary. The only missing binary assessment is the Cr-Ta system, which does not have a stable FCC phase. The self-diffusion mobilities for the Cr and Ta are based on the values established in Co-Cr and Ni-Ta binary assessments, respectively. The diffusivities of Ta in FCC Cr and of Cr in FCC Ta are initially estimated using the work of Xin et al. [25] and then refined using the experimental data for the composition profiles from the Co-0.25 Cr/Co-0.014 Ta and Co/Ni-0.10Ta ternary diffusion couples at 1200 °C (as seen in Figures 10 and 11). In addition, the Ni-Ta/Ni-Cr diffusion couple is used to help validate the end-

members for the FCC Cr and Ta mobility parameters. The results from this couple are also included in the supplement material. After optimization of the impurity diffusivities and the selected binary interaction parameters

(${}^0A_{Ni}^{Cr,Co}$, ${}^0A_{Ni}^{Co,Ta}$, ${}^0A_{Cr}^{Co,Ni}$, ${}^0A_{Cr}^{Co,Ta}$, ${}^0A_{Co}^{Cr,Ni}$, ${}^0A_{Co}^{Cr,Ta}$, ${}^0A_{Ta}^{Co,Cr}$, and ${}^0A_{Ta}^{Co,Ni}$)

Figure 10 shows that good agreement is achieved between the measured and predicted composition profiles. Figure 11 indicates that the agreement between the measured and predicted composition profiles for the Co/Ni-0.10Ta ternary diffusion couple is also acceptable. However, there are some discrepancies between the predicted and measured profile for Ni and Co compositions. The measured Co and Ni diffusivities are faster than predicted at 1200 °C. The same discrepancies were present in the diffusion couple at 1000 °C (see supplemental files for the 1000 °C profile)

Co-Ni-Re

The mobility of Re in FCC-Co was initially estimated using the first-principles values calculated by Naghavi et al [20]. The self-diffusivity for Re in FCC-Re is adopted from the work by Chen et al. [37], which is based on the first-principles simulations by Angsten et. al. [83]. Using these initial estimates, the mobility description and thermodynamic database were used to predict the composition profiles from the ternary diffusion couples, Ni/Ni-0.05 Co- 0.05 Re and Ni- 0.05 Co/Ni-0.05 Re, studied by Mabruri et al. [53] at 1250 °C. The ternary composition profiles were then used to optimize the mobility of Re in FCC-Co (Q_{Co}^{Re}) at 1250 °C using TC-Python. It should be noted that as the diffusion couples were only investigated at a single temperature, the temperature dependence of this mobility was not optimized and remained constant.

The resulting optimization, which is included in Table 4, is the best compromise between the experimental work reported by Neumeier et al. [7] and Mabruri et al. [53] and the available first-principles data. Figure 12 predicts Re diffusivity in FCC-Co as function of temperature and compares this to recent experimental work by Neumeier et al. [7] and to other first-principles predictions [7]. Figure 13 shows the predicted Re interdiffusion coefficient as a function of composition compared to experimental measurements by Neumeier. The current work predicts the correct temperature dependence of the interdiffusion coefficients, but it does not reproduce the increasing diffusivity with the decreasing Re content. Additionally, the diffusivity at 1300 °C is slightly lower than observed. After optimizing the mobility of Co in FCC-Re, the predicted and measured composition profiles for the Ni/Ni-0.05Co-0.05 Re and Ni-0.05Co/Ni-0.05Re diffusion couples are in relatively good agreement, as seen in Figures 14 and 15. For both diffusion couples, there are some discrepancies noted in the predicted Co composition profiles. For the Ni/Ni-0.05Co-0.05Re diffusion couple, the predicted Co diffusivity is slower than observed. Co composition profile predicted for the N-0.05Co/Ni-0.05Re diffusion couple indicated that uphill diffusion was present at the diffusion couple interface; however, this was not observed experimentally. To improve the agreement between the measured and predicted ternary diffusion coupled would require additional adjustment of the Co self-diffusivity in FCC-Co. While the self-diffusivity of Co in FCC-Co was adjusted based on some of the binary Co-Al and Co-W diffusion, additional optimization of the self-diffusivity based on this ternary diffusion couple data was not considered. Adjustment based on this ternary assessment would have required re-adjustment of all the other binary Co systems.

Database validation

To validate the current diffusion mobility database, the composition profiles for a variety of measured ternary, quaternary, quinary diffusion couples were compared to the predictions using current thermodynamic and mobility parameters. The data from these diffusion couples were not included in any of the optimization processes.

The end-member compositions and conditions for the different validation couples are given in Table 5. All the ternary diffusion couples resided in the single γ phase region, unless noted. For the Co-Cr-Ni system, Chen et al. [49] investigated the diffusivities at 1300 °C using seven different diffusion couples. Three of the diffusion couples were chosen for validating the current mobility descriptions and the location of the diffusion couple end-members is shown on the isothermal ternary section at 1300 °C in Figure 16a. Figures 16b, 16c and 16d) show the predicted composition profiles compared with the measured profiles for three of the Co-Cr-Ni diffusion: all of which are in good agreement.

Table 5. Composition and annealing conditions for validation diffusion couples

Diffusion Couple		Annealing Temperature (°C)	Annealing time (h)	Reference	Notes
End-member composition (mole fraction)	End-member composition (mole fraction)				
Co - 0.50 Ni	Co - 0.25 Cr	1300	50	[49]	
Co - 0.25 Ni	Ni - 0.20 Cr	1300	50	[49]	
Ni - 0.40 Cr	Co - 0.20 Ni	1300	50	[49]	
Co - 0.30 Cr	Co - 0.10 Ti	1150	100	[50]	
Co-0/15Cr-0.08Ti	Co	1150	100	[50]	
Co-0.203Cr	Co-0.095W	1100	120	[84]	
Co	Co-0.103Cr-0.07W	1100	120	[84]	
Co-0.06Al-0.279Cr (mass fraction)	Ni-0.053Al-0.348Co (mass fraction)	1100	48	[57]	Co-0.06Al-0.279Cr end-member is in the γ^+ B2 phase region
Co-0.066Al-0.287Cr (mass fraction)	Ni-0.014Al-0.055Cr-0.08.9Ti (mass fraction)	1100	72	[57]	Co-0.066Al-0.287Cr end-member is in the γ^+ B2 phase region

The ternary diffusivities measured by Zhou et al. [50] were used to validate the current mobility descriptions in the Co-Cr-Ti FCC phase. Zhou et al. analyzed seven different diffusion couples in the Co-Cr-Ti system at 1050 °C. Two of these couples (Co-0.30 Cr /Co-0.10 Ti and Co-0.14Cr-0.1Ti /Co) were chosen to compare the predictions using the current mobility

assessments with the measured composition profiles. The location of the end-members for the two diffusion couples are shown in Figure 17a, where the diffusion couple end-members are labelled “A”, “B”, “C” and “D.” All the measured interdiffusion coefficients at 1050 °C are compared to the predicted values in Figure 17b. The best agreement between the measured and predicted coefficients is observed for the Cr interdiffusion in Co, $D_{Cr,Cr}^{Co}$. Figures 17c and 17d show the predicted and measured composition profiles for the two diffusion couples at 1050 °C for 100 h. The predicted and measured compositions are in good agreement.

Validation of the Co-Cr-W system was performed using the data by Zhang et. al. [51]. They measured the diffusivities in four different diffusion couples at 1100 °C for 120 h. The region that includes the four diffusion couples is shown in the isothermal section given by Figure 18a, where the end-member compositions are marked as “A”, “B”, “C” and “D.” Again, all the measured interdiffusion coefficients are compared with the current predicted diffusion coefficient in Figure 18b. There is relatively good agreement between the measured and predicted interdiffusion coefficients, with the best agreement being for the interdiffusion of W in Co, $D_{W,W}^{Co}$. The measured and predicted composition profiles for two of the diffusion couples at 1100 °C are shown in Figure 18c and 18d.

The quaternary and quinary diffusion couples measured by Gómez-Acebo et al [57] provided the final validation of the database. Both of these diffusion couples were annealed at 1100 °C and included one end-member that was a composition in the two phase $\gamma + B2$ region. Simulation of these diffusion profiles included the B2 phase as a precipitate phase with no diffusion. The measured composition profiles are compared to predicted composition profiles for the FCC (γ) phase. Figure 18 compares the measured and predicted composition profiles for the quaternary diffusion couple Co-0.06Al-0.279Cr/Ni-0.053Al-0.348Co (mass fraction) after 48 h at 1100 °C. The Co-0.06Al-0.279Cr (mass fraction) end-member is two phase a $\gamma + B2$ alloy and additional scatter in measured composition data is observed on this side of the diffusion couple. Overall, the agreement between the measured and predicted composition profiles is acceptable. For the quinary diffusion couple in the Co-Cr-Ni-Al-Ti system at 1100 °C, shown in Figure 19, the Co-0.066Al-0.287Cr (mass fraction) end-member is a two-phase mixture of $\gamma + B2$. Again, additional scatter in the experimental data is observed on the side of the two-phase end-member composition. The measured and predicted composition profiles are in relatively good agreement, although there are some discrepancies between the measured and predicted Al composition profiles. The predicted Al composition profile does not indicate as much up-hill diffusion at the interface as observed, indicating that the Al diffusivity may be faster than predicted.

VI. Discussion/Conclusions.

The current assessment approach of combining experimental, first-principles data and diffusion correlations has been effective in developing the multicomponent diffusion mobility descriptions for the Co-Al-Ni-W-Cr-Ta-Ti-Re FCC phase. The multiple composition profiles were collected for each data set and merged to minimize the scatter associated with each composition profile. This improved the optimization process as the simulations could be directly compared to a spline fit of the experimental data. A set of ternary and higher order diffusion couples were designated to validate the assessment and this data was not included in the optimization process. Good

agreement was obtained with a variety of validation diffusion couple data previously reported in the literature and not included in the assessment process. Further validation of the diffusion mobility descriptions is still needed and will include additional diffusion couple experiments focused on the Ti and Re interdiffusion in the FCC matrices and a diffusion couple experiment that includes all the elements in the system.

In an effort, to facilitate the continued development of multicomponent diffusion databases all of the experimental data associated with this work, as well as the published experimental data used in the assessment and validation process are available through the materialdata.nist.gov and the phasedata.nist.gov repositories. With greater access to the data needed to refine assessments and add additional elements the materials science community will be able to develop larger and more robust databases. Access to re-useable data will also support the growing number of tools designed to automate the assessment process.

Acknowledgments

WT acknowledges financial support from awards 70NANB14H012 and 70NANB19H005 from U.S. Department of Commerce, National Institute of Standards and Technology as part of the Center for Hierarchical Materials Design (CHiMaD).

References

- [1] J. Sato, T. Omori, K. Oikawa, I. Ohnuma, R. Kainuma, K. Ishida, Cobalt-Base High-Temperature Alloys, *Science*, 2006, 312, p 90-91. 10.1126/science.1121738
- [2] T. Pollock, J. Dibbern, M. Tsunekane, J. Zhu, A. Suzuki, New Co-based γ - γ' high-temperature alloys, *JOM*, 2010, 62 (1), p 58-63. 10.1007/s11837-010-0013-y
- [3] E.A. Lass, Application of Computational Thermodynamics to the Design of a Co-Ni-Based γ' -Strengthened Superalloy, *Metall. Mater. Trans. A.*, 2017, 48A (5), p. 2443–2459 10.1007/s11661-017-4040-y
- [4] J. Ruan, W. Xu, T. Yang, J. Yu, S. Yang, J. Luan, T. Omori, C. Wang, R. Kainuma, K. Ishida, C.T. Liu, X. Liu, Accelerated design of novel W-free high-strength Co-base superalloys with extremely wide γ/γ' region by machine learning and CALPHAD methods, *Acta Mater.*, 2020, 186, p 425-433. 10.1016/j.actamat.2020.01.004
- [5] P. Liu, H. Huang, S. Antonov, C. Wen, D. Xue, H. Chen, L. Li, Q. Feng, T. Omori, Y. Su, Machine learning assisted design of γ' -strengthened Co-base superalloys with multi-performance optimization, *Comput. Mater.* 2020, 62 (6), <https://doi.org/10.1038/s41524-020-0334-5>
- [6] S.S. Naghavi, V.I. Hegde, A. Saboo, C. Wolverton, Energetics of cobalt alloys and compounds and solute–vacancy binding in fcc cobalt: A first-principles database, *Acta Mater.*, 2017, 124, p 1-8. 10.1016/j.actamat.2016.10.065
- [7] S. Neumeier, H.U. Rehman, J. Neuner, C.H. Zenk, S. Michel, S. Schuwalow, J. Rogal, R. Drautz, M. Göken, Diffusion of solutes in fcc cobalt investigated by diffusion couples and first principles kinetic Monte Carlo, *Acta Mater.*, 2016, 106, p 304-312. 10.1016/j.actamat.2016.01.028

- [8] Center for Hierarchical Materials Design, Northwestern University, Evanston, IL 2022. <https://chimad.northwestern.edu>.
- [9] U.R. Kattner, Construction of a Thermodynamic Database for Ni-base Superalloys: A Case Study, in: P.E.A. Turchi, A. Gonis, R.D. Shull (Eds.) TMS, Warrendale, PA, 2002, pp. 147-164.
- [10] P. Wang, W. Xiong, U.R. Kattner, C.E. Campbell, E.A. Lass, O.Y. Kontsevoi, G.B. Olson, Thermodynamic re-assessment of the Al-Co-W system, *Calphad*, 2017, 59, p 112-130. [10.1016/j.calphad.2017.09.007](https://doi.org/10.1016/j.calphad.2017.09.007)
- [11] P. Wang, M.C. Peters, U.R. Kattner, K. Choudhary, G.B. Olson, Thermodynamic analysis of the topologically close packed sigma phase in the Co-Cr system, *Intermetallics*, 2019, 105, p. 13-20. [10.1016/j.intermet.2018.11.004](https://doi.org/10.1016/j.intermet.2018.11.004)
- [12] P. Wang, O.Y. Kontsevoi, G.B. Olson, Thermodynamic analysis of the Co-W System *J. Mater. Sci.*, 2019, 54, p 10261-10269. <https://doi.org/10.1007/s10853-019-03616-3>
- [13] P. Wang, T. Hammerschmidt, U.R. Kattner, G.B. Olson, Structural stability of Co-V intermetallic phases and thermodynamic description of the Co-V system, *CALPHAD*, 2020, 68, p 7. <https://doi.org/10.1016/j.calphad.2019.101729>
- [14] P. Wang, J. Koßmann, U.R. Kattner, M. Palumbo, T. Hammerschmidt, G.B. Olson, Thermodynamic assessment of the Co-Ta system, *CALPHAD*, 2019, 64, p 205-212. <https://doi.org/10.1016/j.calphad.2018.12.002>
- [15] C.E. Campbell, W.J. Boettinger, U.R. Kattner, Development of a diffusion mobility database for Ni-base superalloys, *Acta Mater.*, 2002, 50 (4), p 775-792.
- [16] C.E. Campbell, NIST Ni-based diffusion mobility database, materialsdata.nist.gov, 2008, <http://hdl.handle.net/11256/942>.
- [17] J. Ågren, Numerical Treatment of Diffusional Reactions in Multicomponent Alloys, *J. Phys. Chem. Solids*, 1982, 43(4), p 385-391.
- [18] J. Ågren, Diffusion in Phases with Several Components and Sublattices, *J. Phys. Chem. Solids*, 1982, 43(5), p 421-430.
- [19] F. Liu, Z. Wang, Z. Wang, J. Zhong, X. Wu, Z. Qun, Z. Li, L. Tan, L. Zhao, L. Zhu, L. Jiang, L. Huang, L. Zhang, Y. Liu, High-throughput determination of interdiffusivity matrices in Ni-Al-Ti-Cr-Co-Mo-Ta-W multicomponent superalloys and their application in optimization of creep resistance, *Mater. Today Commun.*, 2020, 24, p 11. <https://doi.org/10.1016/j.mtcomm.2020.101018>
- [20] S.S. Naghavi, V.I. Hegde, C. Wolverton, Diffusion coefficients of transition metals in fcc cobalt, *Acta Mater.*, 2017, 132, p 467-478. <http://dx.doi.org/10.1016/j.actamat.2017.04.060>
- [21] J. Askill, *Tracer Diffusion Data for Metals, Alloys and Simple Oxides*, Plenum, New York, 1970.
- [22] A.D. Le Claire, On the theory of impurity diffusion in metals, *Philos.Mag.*, 1962, 7(73), p 141-167. [10.1080/14786436208201866](https://doi.org/10.1080/14786436208201866)
- [23] A.M. Brown, M.F. Ashby, Correlations for Diffusion Constants, *Acta Metall.*, 1980, 28, p 1085-1101.
- [24] J. Cahoon, O.D. Sherby, The Activation Energy for Lattice Self-Diffusion and the Engel-Brewer Theory, *Metall. Trans. A*, 1992, 23A(9), p 2491-2500.
- [25] J. Xin, Y. Du, S.-L. Shang, A New Relationship Among Self- and Impurity Diffusion Coefficients in Binary Solution Phases, *Metall. Mater. Trans.*, 2016, 47A(7), p 3295-3299.

- [26] G. Erdélyi, D.L. Beke, F.J. Kedves, I. Gödény, Determination of diffusion coefficients of Zn, Co and Ni in aluminium by a resistometric method, *Philos. Mag. B*, 1978, 38(5), p 445-462. [10.1080/13642817808246394](https://doi.org/10.1080/13642817808246394)
- [27] K.-I. Hirano, R.P. Agarwala, M. Cohen, Diffusion of Iron, Nickel and Cobalt in Aluminum, *Acta Metall.*, 1962, 10(9), p 857-863.
- [28] A. Davin, V. Leroy, D. Coutouradis, L. Habraken, Comparison of the Diffusion of Some Substitution Elements in Nickel and Cobalt, *Cobalt*, 1963, 19(6), p 51-56.
- [29] J.W. Weeton, Diffusion Of Chromium In Alpha Cobalt-Chromium Solid Solutions, National Advisory Committee For Aeronautics, Washington DC, 1951, p. 22.
- [30] V.D. Divya, U. Ramamurty, A. Paul, Diffusion in Co-Ni System Studied by Multifoil Technique, *Def. Diff. For.*, 2011, 312-315, p 466-471.
<https://doi.org/10.4028/www.scientific.net/DDF.312-315.466>
- [31] Y.W. Cui, M. Jiang, I. Ohnuma, K. Oikawa, R. Kainuma, K. Ishida, Computational study of atomic mobility for fcc phase of Co-Fe and Co-Ni binaries, *J. Phase Equilib. Diffus.*, 2008, 29(1), p 2-10. [10.1007/s11669-007-9238-z](https://doi.org/10.1007/s11669-007-9238-z)
- [32] K.-I. Hirano, R.P. Agarwala, B.L. Averbach, M. Cohen, Diffusion in Cobalt-Nickel Alloys, *J. Appl. Physics*, 1962, 33(10), p 3049-3054.
- [33] H. Liu, Y. Liu, Y. Du, Q. Min, J. Zhang, S. Liu, Atomic mobilities and diffusivities in fcc Co-X (X=Mn, Pt and Re) alloys, *CALPHAD*, 2019, 64, p 306-312.
<https://doi.org/10.1016/j.calphad.2019.01.003>
- [34] P.J.M. van der Straten, G.F. Bastin, F.J.J. van Loo, G.D. Rieck, Phase Equilibria and Interdiffusion in the Cobalt-Titanium System, *Z. Met.kd.*, 1975, 67, p 152-157.
- [35] Y.W. Cui, G. Xu, R. Kato, X.-G. Lu, R. Kainuma, K. Ishida, Interdiffusion and Atomic Mobility for FCC-Centered Cubic (FCC) Co-W Alloys, *Metall. Mater. Trans. A*, 2013, 44A(4), p 5. [10.1007/s11661-012-1586-6](https://doi.org/10.1007/s11661-012-1586-6)
- [36] S.M. Klotsman, S.V. Osetrov, A.N. Timofeev, Volume diffusion of cobalt in tungsten single crystal, *Physical Review B*, 1997, 46(5), p 2831-2837.
- [37] J. Chen, J. Zhao, L. Zhang, X.-G. Lu, L. Liu, Atomic mobilities in fcc Ni-rich Ni-X (X=Rh, Ta, W, Re, and Ir) systems, *CALPHAD*, 2019, 65, p 316-325.
<https://doi.org/10.1016/j.calphad.2019.03.013>
- [38] M.S.A. Karunaratne, P. Carter, R.C. Reed, Interdiffusion in the fcc-centred cubic phase of the Ni-Re, Ni-Ta, and Ni-W systems between 900 and 1300 °C, *Mater. Sci. Eng.*, 2000, A281, p 229-233.
- [39] W.J. Boettinger, M.E. Williams, K.W. Moon, G.B. McFadden, P.N. Patrone, J.H. Perepezko, Interdiffusion in the Ni-Re System: Evaluation of Uncertainties, *J. Phase Equilib. Diffus.*, 2017, 38(5), p 750-763. [10.1007/s11669-017-0562-7](https://doi.org/10.1007/s11669-017-0562-7)
- [40] M. Liu, L. Zhang, W. Chen, J. Xin, Y. Du, H. Xu, Diffusivities and atomic mobilities in fcc Al Ni-X (X=Ge, Ti and V) alloys, *Calphad*, 2013, 41, p 108-118.
[10.1016/j.calphad.2013.02.005](https://doi.org/10.1016/j.calphad.2013.02.005)
- [41] G.W. Roper, D.P. Whittle, Interdiffusion in ternary Co-Cr-Al, *Metal Science*, 1980, (1), p 21-28.
- [42] Y. Wang, N. Zhu, H. Wang, X.-G. Lu, Interdiffusion and Diffusion Mobility for fcc Ni-Co-Al Alloys, *Metall. Mater. Trans. A*, 2017, 48A, p 943-947. [10.1007/s11661-016-3908-6](https://doi.org/10.1007/s11661-016-3908-6)
- [43] L. Zhu, C. Wei, H. Qi, L. Jiang, Z. Jin, J.-C. Zhao, Experimental investigation of phase equilibria in the Co-rich part of the Co-Al-X (X = W, Mo, Nb, Ni, Ta) ternary systems using

- diffusion multiples, *J. Alloys Compd.*, 2017, 691, p 110-118.
<http://dx.doi.org/10.1016/j.jallcom.2016.08.210>
- [44] Y. Chen, J. Li, B. Tang, G. Xu, H. Kou, Y. Cui, Interdiffusion in FCC Co-Al-Ti Ternary Alloys, *J Phase Equil and Diffus.*, 2015, 36, p 127-135. DOI: 10.1007/s11669-015-0367-5
- [45] K.-W. Moon, C.E. Campbell, M.E. Williams, W.J. Boettinger, Diffusion in FCC Co-rich Co-Al-W Alloys at 900 and 1000 °C, *J. Phase. Equilib. Diffus.*, 2016, 37(4), p 402-415. 10.1007/s11669-016-0486-7
- [46] H. Chang, G. Xu, X.-G. Lu, L. Zhou, K. Ishida, Y. Cui, Experimental and phenomenological investigations of diffusion in Co–Al–W alloys, *Scripta Mater.* 2015, 106, p 13-16. 10.1016/j.scriptamat.2015.03.021
- [47] S. Obata, M. Moniruzzaman, Y. Murata, Interdiffusion in Co-Based Co-Al-W Ternary Alloys at Elevated Temperatures, *ISIJ International*, 2014, 54(10), p 2129-2133. 10.2355/isijinternational.54.2129
- [48] J. Chen, J. Xiao, Z. Lu, C. Wang, L. Zhang, Atomic mobilities and interdiffusivities in Ni-rich fcc Ni-Co-Cr and Ni-Al-Co-Cr systems evaluated using composition profiles and HitDIC, *J. Alloy. Compd.*, 2021, 865, p 158645.
<https://doi.org/10.1016/j.jallcom.2021.158645>
- [49] J. Chen, Y. Liu, G. Sheng, F. Lei, Z. Kang, Atomic mobilities, interdiffusivities and their related diffusional behaviors in fcc Co–Cr–Ni alloys, *J. Alloy. Compd.*, 2015, 621, p 428-433. 10.1016/j.jallcom.2014.09.139
- [50] Z. Zhou, Y. Liu, Atomic Mobilities and Diffusivities in fcc Co-Cr-Ti Alloys, *J. Phase Equil. Diffus.*, 2016, 37, p 155-161. 10.1007/s11669-015-0437-8
- [51] W. Zhang, D. Liu, L. Zhang, Y. Du, B.-y. Huang, Experimental investigation and computational study of atomic mobility in fcc ternary Co–Cr–W alloys, *CALPHAD*, 2014, 45, p 118-126. <http://dx.doi.org/10.1016/j.calphad.2013.11.005>
- [52] J. Huang, Y. Wang, J. Wang, X.-G. Lu, L. Zhang, Thermodynamic Assessments of the Ni-Cr-Ti System and Atomic Mobility of Its fcc Phase, *J. Phase Equilib. Diffus.*, 2018, 39, p 597-609. <https://doi.org/10.1007/s11669-018-0650-3>
- [53] E. Maburri, S. Sakurai, Y. Murata, T. Koyama, M. Morinaga, Interdiffusion in Ni-Co-Re and Ni-Co-Ru systems, *Mater. Trans.*, 2007, 48(10), p 2718-2723. 10.2320/matertrans.MRA2007116
- [54] X.J. Liu, J.Y. Lin, Y. Lu, Y.H. Guo, C.P. Wang, Assessment of the atomic mobility for the fcc phase of Ni–Co–X (X- Re and Ru) system, *CALPHAD*, 2014, 45, p 138-144.
<http://dx.doi.org/10.1016/j.calphad.2013.12.003>
- [55] V.D. Divya, U. Ramamurty, A. Paul, Interdiffusion and Growth of the Phases in CoNi/Mo and CoNi/W Systems, *Metall. Materials Trans.*, 2012, 43A, p. DOI: 10.1007/s11661-011-0990-7
- [56] Y. Minamino, Y. Koizumi, N. Tsuji, T. Yamada, T. Takahashi, Interdiffusion in Co solid solutions of Co-Al-Cr-Ni system at 1423 K, *Mater. Trans.*, 2003, 44(1), p 63-71. 10.2320/matertrans.44.63
- [57] T. Gómez-Acedbo, B. Navarcorena, F. Castro, Interdiffusion in Multiphase, Al-Co-Cr-Ni-Ti Diffusion Couples, *J. Phase Equilib. Diffus.*, 2004, 25 (3), p 237-251.
- [58] F. Liu, Z. Wang, Z. Wang, J. Zhong, X. Wu, Z. Qin, Z. Li, L. Tan, L. Zhao, L. Zhu, L. Jiang, L. Huang, L. Zhang, Y. Liu, High-throughput determination of interdiffusivity matrices in Ni-Al-Ti-Cr-Co-Mo-Ta-W multicomponent superalloys and their application in

- optimization of creep resistance, *Mater.Today Commun.*, 2020, 24, p. 10.1016/j.mtcomm.2020.101018
- [59] M. Walbrühl, A. Blomqvist, P.A. Korzhavyi, C.M. Araujo, Surface gradients in cemented carbides from first-principles-based multiscale modeling: Atomic diffusion in liquid Co, *Int. J. Refract. Met. Hard Mater.*, 2017, 66, p 174-179. 10.1016/j.ijrmhm.2017.03.016
- [60] A. Borgenstam, A. Engström, L. Höglund, J. Ågren, DICTRA, a Tool for Simulation of Diffusion Transformations in Alloys, *J. Phase Equilib.*, 2000, 21(3), p 269-280.
- [61] J.O. Andersson, T. Helander, L. Höglund, P.F. Shi, B. Sundman, Thermo-Calc and DICTRA, *Computational tools for materials science, CALPHAD*, 2002, 26, p 273-312.
- [62] J. Zhong, L. Chen, L. Zhang, Automation of diffusion database development in multicomponent alloys from large number of experimental composition profiles, *npj Comput. Mater.*, 2021, 7(1), p 35. 10.1038/s41524-021-00500-0
- [63] K. Abrahams, S. Zomorodpoosh, A.R. Khorasgani, I. Roslyakova, I. Steinbach, J. Kundin, Automated assessment of a kinetic database for fcc Co–Cr–Fe–Mn–Ni high entropy alloys, *Model. Simul. Mater. Sci. Eng.*, 2021, 29(5), p 055007. 10.1088/1361-651x/abf62b
- [64] DICTRA, Thermo-Calc AB, Stockholm, Sweden, 2003.
- [65] TC-Python, Thermo-Calc Software AB, Stockholm, Sweden, 2021.
- [66] A. Salmasi, S.J. Graham, I. Galbraith, A.D. Graves, M. Jackson, S. Norgren, D. Guan, H. Larsson, L. Höglund, Mobilities of Ti and Fe in disordered TiFe-BCC assessed from new experimental data, *Calphad*, 2021, 74, p 102300. <https://doi.org/10.1016/j.calphad.2021.102300>
- [67] C.E. Campbell, A.L. Rukhin, Evaluation of self-diffusion data using weighted means statistics, *Acta Mater.*, 2011, 59(13), p 5194-5201. 10.1016/j.actamat.2011.04.055
- [68] Y.W. Cui, M. Jiang, I. Ohnuma, K. Oikawa, R. Kainuma, K. Ishida, Computational study of atomic mobility in Co-Fe-Ni ternary fcc alloys, *J. Phase Equilib. Diffus.*, 2008, 29(4), p 312-321. 10.1007/s11669-008-9341-9
- [69] R.C. Ruder, C.E. Birchenall, Cobalt Self-Diffusion: A Study of the Method of Decrease in Surface Activity, *JOM*, 1951, 3(2), p 142-146. 10.1007/BF03397290
- [70] B. Million, J. Kucera, Concentration Dependence of Nickel Diffusion in Nickel-Cobalt Alloys, *Czech. J. Phys. B*, 1971, B 21(2), p 161-171.
- [71] W. Bussmann, C. Herzig, W. Rempp, K. Maier, H. Mehrer, Isotope Effect and Self-Diffusion in Face-Centred Cubic Cobalt, *Phys. Stat. Solid.A*, 1979, 56, p 87-97.
- [72] C.G. Lee, Y. Iijima, K. Hirano, Self-Diffusion and Isotope Effect in Face-Centred Cubic Cobalt, *Def. Diff. For.*, 1993, 95-98, p 723-728. <https://doi.org/10.4028/www.scientific.net/DDF.95-98.723>
- [73] B. Jonsson, Assessment of the Mobilities of Cr, Fe and Ni in Binary Fcc Cr-Fe and Cr-Ni Alloys, *Scand. J. Metall.*, 1995, 24(1), p 21-27.
- [74] A.T. Dinsdale, Sgte Data for Pure Elements, *CALPHAD*, 1991, 15(4), p 317-425.
- [75] S. Yang, Y. Wang, Z.-K. Liu, Y. Zhong, Ab initio simulations on the pure Cr lattice stability at 0K: Verification with the Fe-Cr and Ni-Cr binary systems, *Calphad*, 2021, 75, p. 10.1016/j.calphad.2021.102359
- [76] Y.W. Cui, K. Oikawa, R. Kainuma, K. Ishida, Study of diffusion mobility of Al-Zn solid solution, *J. Phase Equilib. Diffus.*, 2006, 27(4), p 333-342. 10.1361/154770306x116261
- [77] J. Chen, J. Xiao, Z. Lu, C. Wang, L. Zhang, Atomic mobilities and interdiffusivities in Ni-rich fcc Ni-Co-Cr and Ni-Al-Co-Cr systems evaluated using composition profiles and HitDIC, *J.Alloys Compd.*, 2021, 865, p. 10.1016/j.jallcom.2021.158645

- [78] S.B. Jung, T. Yamane, Y. Minamino, K. Hirao, H. Araki, S. Saji, Interdiffusion and its size effect in nickel solid solutions of Ni-Co, Ni-Cr and Ni-Ti systems, *J.Mater. Sci. Lett.*, 1992, 11, p 1333-1337.
- [79] N. Komai, M. Watanage, Z. Hortia, T. Sano, M. Nemoto, Analytical Electron Microscopy Study of Ni/Ni-8 Mol% Ti Diffusion Couples, *Acta Mater.*, 1998, 40(12), p 4443-4451.
- [80] M.S.A. Karunaratne, P. Carter, R.C. Reed, On the diffusion of aluminium and titanium in the Ni-rich Ni-Al-Ti system between 900 and 1200 degrees C, *Acta Mater.*, 2001, 49(5), p 861-875.
- [81] Z. Zhou, Y. Liu, G. Sheng, F. Lei, Z. Kang, A contribution to the Ni-based mobility database: Fcc Ni-Fe-Ti ternary alloy, *Calphad*, 2015, 48, p 151-156.
10.1016/j.calphad.2014.12.003
- [82] J. Zhang, Y. Du, Y. Liu, W. Zhang, D. Liu, C. Chen, Assessment of atomic mobilities for fcc Co-Ti-V alloys, *Calphad*, 2018, 61, p 179-188. 10.1016/j.calphad.2018.04.002
- [83] T. Angsten, T. M. Ayeshiba, H. Wu, D. Morgan, Elemental vacancy diffusion database from high-throughput first-principles calculations for fcc and hcp structures, *New Journal of Physics*, 2014, 16, p 015018. doi:10.1088/1367-2630/16/1/015018
- [84] W.B. Zhang, D.D. Liu, L.J. Zhang, Y. Du, B.Y. Huang, Experimental investigation and computational study of atomic mobility in fcc ternary Co-Cr-W alloys, *Calphad*, 2014, 45, p 118-126.

Table 4. Mobility parameters for the FCC phase for Co-Al-W-Ni-Cr-Re-Ti-Ta-W*

Parameter		Value	Reference
Mobility of Al			
(FCC,Al:VA;0)	Q_{Al}^{Al}	-126719 - 95.09*T	[76]
(FCC,Co:VA;0)	Q_{Al}^{Co}	304078 - 53.19*T	This work; [46]
(FCC,Cr:VA;0)	Q_{Al}^{Cr}	-261719 - 89.06*T	This work
(FCC,Ni:VA;0)	Q_{Al}^{Ni}	-254235 - 80.59*T	This work
(FCC,Re:VA;0)	Q_{Al}^{Re}	-284000 - 59.82*T	[18]
(FCC,Ta:VA;0)	Q_{Al}^{Ta}	-263875 - 68.97*T	This work
(FCC,Ti:VA;0)	Q_{Al}^{Ti}	-515852 - 5.77*T	[18]
(FCC,W:VA;0)	Q_{Al}^W	-316214 - 73.28*T	This work; [46]
FCC,Al,Co:VA;0	${}^0A_{Al}^{Al,Co}$	-65424 - 35.60*T	This work
FCC,Al,Cr:VA;0	${}^0A_{Al}^{Al,Cr}$	-330259 - 60.71*T	This work
FCC,Al,Ni:VA;0	${}^0A_{Al}^{Al,Ni}$	-125264 - 54.81*T	This work
FCC,Al,Ta:VA;0	${}^0A_{Al}^{Al,Ta}$	-260586 - 35.8*T	This work
FCC,Al,W:VA;0	${}^0A_{Al}^{Al,W}$	-146427 - 16.11*T	This work
FCC,Co,Cr:VA;0	${}^0A_{Al}^{Co,Cr}$	-10092 - 29.92*T	This work
FCC,Co,Ta:VA;0	${}^0A_{Al}^{Co,Ta}$	135887 - 24.04*T	This work
FCC,Co,Ti:VA;0	${}^0A_{Al}^{Co,Ti}$	+ 278731	This work
FCC,Cr,Ni:VA;0	${}^0A_{Al}^{Cr,Ni}$	-55206 + 28.17*T	This work
FCC,Ni,Ti:VA;0	${}^0A_{Al}^{Ni,Ti}$	116464 - 80.1*T	[15, 16]
Mobility of Co			
(FCC,Al:VA;0)	Q_{Co}^{Al}	-175053 - 25.94*T	This work [46]
(FCC,Co:VA;0)	Q_{Co}^{Co}	-301795 - 72.25*T	This work; [46]
(FCC,Cr:VA;0)	Q_{Co}^{Cr}	-264517-83.44*T	This work
(FCC,Ni:VA;0)	Q_{Co}^{Ni}	-267493 - 82.21*T	This work
(FCC,Re:VA;0)	Q_{Co}^{Re}	-457993.7 - 98.8*T	This work
(FCC,Ta:VA;0)	Q_{Co}^{Ta}	-249904 - 66.58*T	This work
(FCC,Ti:VA;0)	Q_{Co}^{Ti}	-284169 - 67.65*T	[15, 16]
(FCC,W:VA;0)	Q_{Co}^W	-308714 - 71.85*T	This work; [46]
FCC,Co,Al:VA;0	${}^0A_{Co}^{Al,Co}$	-128693 - 48.00*T	This work
FCC,Co,Cr:VA;0	${}^0A_{Co}^{Co,Cr}$	-38952 - 12.33*T	This work
FCC,Co,Ta:VA;0	${}^0A_{Co}^{Co,Ta}$	-134078 - 25.36*T	This work
FCC,Co,W:VA;0	${}^0A_{Co}^{Co,W}$	-51308 - 20.62*T	This work
FCC,Al,Cr:VA;0	${}^0A_{Co}^{Al,Cr}$	+167829 + 67.97*T	This work
FCC,Cr,Ni:VA;0	${}^0A_{Co}^{Cr,Ni}$	-31597 - 10.49*T	This work
FCC,Al,Ta:VA;0	${}^0A_{Co}^{Al,Ta}$	-21200 - 16.0*T	This work
FCC,Cr,Ta:VA;0	${}^0A_{Co}^{Cr,Ta}$	-31405 - 17.62*T	This work
Mobility of Cr			

(FCC,Al:VA;0)	Q_{Cr}^{Al}	-220771 - 59.78*T	This work
(FCC,Co:VA;0)	Q_{Cr}^{Co}	-284635 - 75.45*T	This work
(FCC,Cr:VA;0)	Q_{Cr}^{Cr}	-235000 - 82*T	[73]
(FCC,Ni:VA;0)	Q_{Cr}^{Ni}	-287908 - 65.60*T	This work
(FCC,Re:VA;0)	Q_{Cr}^{Re}	-287000 - 64.4*T	[15, 16]
(FCC,Ta:VA;0)	Q_{Cr}^{Ta}	-280344 - 62.30*T	This work
(FCC,Ti:VA;0)	Q_{Cr}^{Ti}	-287000 - 64.4*T	[15, 16]
(FCC,W:VA;0)	Q_{Cr}^W	-286522 - 65.22*T;	This work
FCC,Al,Cr:VA;0	${}^0A_{Cr}^{Al,Co}$	-413224 - 54.99*T	This work
FCC,Co,Cr:VA;0	${}^0A_{Cr}^{Co,Cr}$	-67581 - 9.58*T	This work
FCC,Cr,Ni:VA;0	${}^0A_{Cr}^{Cr,Ni}$	-43518 - 9.53*T	This work
FCC,Cr,Ta:VA;0	${}^0A_{Cr}^{Co,Ta}$	-164153 - 18.77*T	This work
FCC,Cr,W:VA;0	${}^0A_{Cr}^{Co,W}$	-166030 - 20.87*T	This work
FCC,Al,Ni:VA;0	${}^0A_{Cr}^{Al,Ni}$	5209.72	This work
FCC,Co,Ni:VA;0	${}^0A_{Cr}^{Co,Ni}$	-8119 - 6.65*T	This work
FCC,Co,Ta:VA;0	${}^0A_{Cr}^{Co,Ta}$	-27697 - 14.34*T	This work
FCC,Co,Ti:VA;0	${}^0A_{Cr}^{Co,Ti}$	+421042	This work
FCC,Cr,W:VA;0	${}^0A_{Cr}^{Cr,W}$	-45072 - 50.46*T	This work
FCC,Ni,W:VA;0	${}^0A_{Cr}^{Ni,W}$	-108080 - 34.36*T	This work
Mobility of Ni			
(FCC,Al:VA;0)	Q_{Ni}^{Al}	-142826 - 56.27*T	This work; [46]
(FCC,Co:VA;0)	Q_{Ni}^{Co}	-272406 - 91.62*T	This work; [46]
(FCC,Cr:VA;0)	Q_{Ni}^{Cr}	-277417 - 54.27*T	This work
(FCC,Ni:VA;0)	Q_{Ni}^{Ni}	-287000 - 77.93*T	[73]
(FCC,Re:VA;0)	Q_{Ni}^{Re}	-229001 - 213*T [‡]	[40]
(FCC,Ta:VA;0)	Q_{Ni}^{Ta}	-263393 - 63.22*T	This work
(FCC,Ti:VA;0)	Q_{Ni}^{Ti}	-352179 - 97*T	[15,16]
(FCC,W:VA;0)	Q_{Ni}^W	-303688 - 77.81*T	This work; [46]
FCC,Al,Ni:VA;0	${}^0A_{Ni}^{Al,Ni}$	-15248 - 70.95*T	This work
FCC,Cr,Ni:VA;0	${}^0A_{Ni}^{Cr,Ni}$	-70283 - 8.42*T	This work
FCC,Ni,Ta:VA;0	${}^0A_{Ni}^{Ni,Ta}$	-177238 - 13.27*T	This work
FCC,Ni,Ti:VA;0	${}^0A_{Ni}^{Ni,Ti}$	-949954 + 62*T	[15,16]
FCC,Ni,W:VA;0	${}^0A_{Ni}^{Ni,W}$	-187110 - 18.96*T	This work
FCC,Al,Ti:VA;0	${}^0A_{Ni}^{Al,Ti}$	38176 + 4.91*T	[15,16]
FCC,Co,Cr:VA;0	${}^0A_{Ni}^{Cr,Co}$	-105013 - 24.42*T	This work
FCC,Co,Ta:VA;0	${}^0A_{Ni}^{Co,Ta}$	410489 + 55.83*T	This work
FCC,Cr,W:VA;0	${}^0A_{Ni}^{Cr,W}$	-70127 - 38.59*T	This work

[‡] Alternate Chen et al. [38] = -457520-71.88*T; based evaluation Re self-diffusion in FCC.

FCC,Ta,W:VA;0	${}^0A_{Ni}^{Ta,W}$	-176400 - 22.03*T	This work
Mobility of Re			
(FCC,Al:VA;0)	Q_{Re}^{Al}	-278817 - 105.2*T	[15]
(FCC,Co:VA;0)	Q_{Re}^{Co}	-278817 - 105.2*T	[15]
(FCC,Cr:VA;0)	Q_{Re}^{Cr}	-278817 - 105.2*T	[15]
(FCC,Ni:VA;0)	Q_{Re}^{Ni}	-314900 - 70.86*T [§]	[40]
(FCC,Re:VA;0)	Q_{Re}^{Re}	-457520 - 71.88*T	[38]
(FCC,Ta:VA;0)	Q_{Re}^{Ta}	-278817 - 105.2*T	[15]
(FCC,Ti:VA;0)	Q_{Re}^{Ti}	-278817 - 105.2*T	[15]
(FCC,W:VA;0)	Q_{Re}^W	-278817 - 105.2*T	[15]
Mobility of Ta			
(FCC,Al:VA;0)	Q_{Ta}^{Al}	-255002 - 46.57*T	This work
(FCC,Co:VA;0)	Q_{Ta}^{Co}	-273310 - 74.99*T	This work
(FCC,Cr:VA;0)	Q_{Ta}^{Cr}	-269835 - 83.52*T	This work
(FCC,Ni:VA;0)	Q_{Ta}^{Ni}	-255289 - 89.0*T	This work
(FCC,Re:VA;0)	Q_{Ta}^{Re}	-255289 - 90.08*T	This work
(FCC,Ta:VA;0)	Q_{Ta}^{Ta}	-267428 - 78.51*T	This work
(FCC,Ti:VA;0)	Q_{Ta}^{Ti}	-267729 - 79.94*T	[15,16]
(FCC,W:VA;0)	Q_{Ta}^W	-275500 - 66.48*T	This work
Mobility of Al, Co, Cr, Ni, W in Ta			
FCC,Al,Ta:VA;0	${}^0A_{Ta}^{Al,Ta}$	-235007 - 28.77*T	This work
FCC,Co,Ta:VA;0	${}^0A_{Ta}^{Co,Ta}$	-91454 - 19.19*T	This work
FCC,Cr,Ta:VA;0	${}^0A_{Ta}^{Cr,Ta}$	-172901 - 20.95*T	This work
FCC,Ni,Ta:VA;0	${}^0A_{Ta}^{Ni,Ta}$	-87500 - 8.94*T	This work
Mobility of Al, Co, Cr, Ni, W in Ta (continued)			
FCC,Al,Co:VA;0	${}^0A_{Ta}^{Al,Co}$	-21500 - 40.39*T	This work
FCC,Co,Cr:VA;0	${}^0A_{Ta}^{Co,Cr}$	-9488 - 10.93*T	This work
FCC,Co,Ni:VA;0	${}^0A_{Ta}^{Co,Ni}$	-36115 - 19.27*T	This work
FCC,Ni,W:VA;0	${}^0A_{Ta}^{Ni,W}$	-288884 - 26.8*T	This work
Mobility of Ti			
(FCC,Al:VA;0)	Q_{Ti}^{Al}	-257818 - 72.77*T	[15,16]
(FCC,Co:VA;0)	Q_{Ti}^{Co}	-255342.04 - 84.16*T	This work
(FCC,Cr:VA;0)	Q_{Ti}^{Cr}	-257090 - 77.87*T	[15,16]
(FCC,Ni:VA;0)	Q_{Ti}^{Ni}	-257090 - 77.87*T	[15,16]
(FCC,Re:VA;0)	Q_{Ti}^{Re}	-254024 - 79.39*T	[15,16]
(FCC,Ta:VA;0)	Q_{Ti}^{Ta}	-257090 - 77.87*T	[15,16]
(FCC,Ti:VA;0)	Q_{Ti}^{Ti}	-261183 - 75.82*T	[15,16]
(FCC,W:VA;0)	Q_{Ti}^W	-257090 - 77.87*T	[15,16]
Mobility of Al, Co, Cr, Ni, W in Ti			
FCC,Al,Ti:VA;0	${}^0A_{Ti}^{Al,Ti}$	-135255 + 20.4*T	[15,16]
FCC,Al,Co:VA;0	${}^0A_{Ti}^{Al,Co}$	103415	This work

[§] Alternate from Chen et al. [38] = -282529.6-99.6*T

FCC,Ni,Ti:VA;0	${}^0A_{Ti}^{Ni,Ti}$	-23949 - 33.6*T	[15,16]
FCC,Al,Ni:VA;0	${}^0A_{Ti}^{Al,Ni}$	-10893	[15,16]
FCC,Co,Cr:VA;0	${}^0A_{Ti}^{Cr,Co}$	+ 22117	This work
Mobility of W			
(FCC,Al:VA;0)	Q_W^{Al}	-285906 - 91.45*T	This work, [46]
(FCC,Co:VA;0)	Q_W^{Co}	-305970 - 63.26*T	This work, [46]
(FCC,Cr:VA;0)	Q_W^{Cr}	-277167 - 85.71*T	This work
(FCC,Ni:VA;0)	Q_W^{Ni}	-296236 - 78.06*T	This work
(FCC,Re:VA;0)	Q_W^{Re}	-282130 - 87.16*T	[15]
(FCC,Ta:VA;0)	Q_W^{Ta}	-211296 - 84.92*T	This work
(FCC,Ti:VA;0)	Q_W^{Ti}	-282130 - 87.16*T	[15]
(FCC,W:VA;0)	Q_W^W	-310679 - 67.73*T	This work, [46]
FCC,Al,W:VA;0	${}^0A_W^{Al,W}$	-88409 - 17.99*T	This work
FCC,Co,W:VA;0	${}^0A_W^{Co,W}$	-178667 - 19.42*T	This work
FCC,Cr,W:VA;0	${}^0A_W^{Cr,W}$	-178753 - 8.46*T	This work
FCC,Ni,W:VA;0	${}^0A_W^{Ni,W}$	-237609 - 25.43*T	This work
FCC,Ta,W:VA;0	${}^0A_W^{Ta,W}$	-57400 - 9.03*T	This work
FCC,Cr,Co:VA;0	${}^0A_W^{Cr,Co}$	-33150 - 30.88*T	This work
FCC,Cr,Ni:VA;0	${}^0A_W^{Cr,Ni}$	+6670 + 9.65*T	This work
FCC,Ni,Ta:VA;0	${}^0A_W^{Ni,Ta}$	-57400 - 9.03 *T	This work

* Corresponding database file is available at materialsdata.nist.gov (<https://hdl.handle.net/11256/998>)

1	2	3	4	5	6	7	8	9	10	11	12	13	14	15	16	17	18	19	20	21
Co -Ta	Co	Co -Cr	Co -Ta	Co -Al	Co -Cr	Co -W	Co -Ta	Ni - Ta	Ni	Ni - Al	Ni - W	Ni - Ta	Ni - Al	Ni - Cr	Co	Ni - Ta	Ni - Cr	Ni - W	Ni	Ni - Cr

Figure 1. Schematic of diffusion couple stack used.

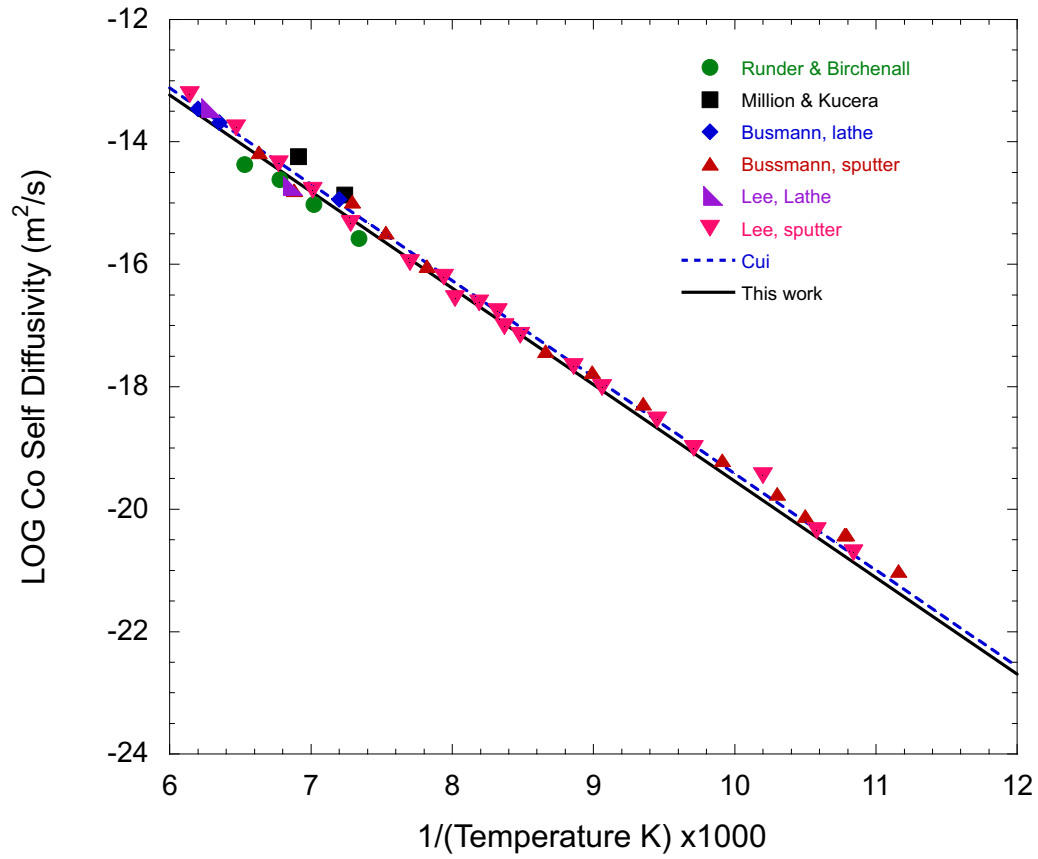


Figure 2. Co self-diffusion measurements [69-72] in comparison to recent assessments [31].

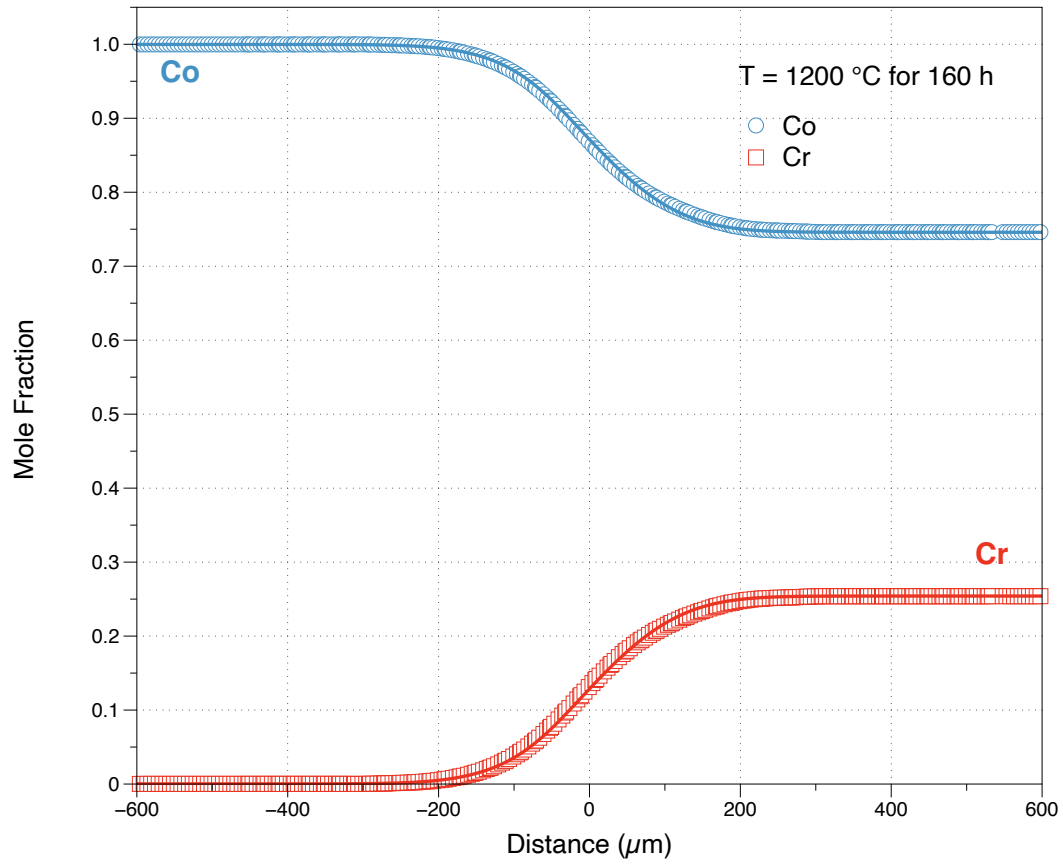


Figure 3. Co/Co-0.25Cr mole fraction composition profiles after 160 h at 1200 °C. Measured compositions are denoted by the open symbols and the solid lines are the predictions.

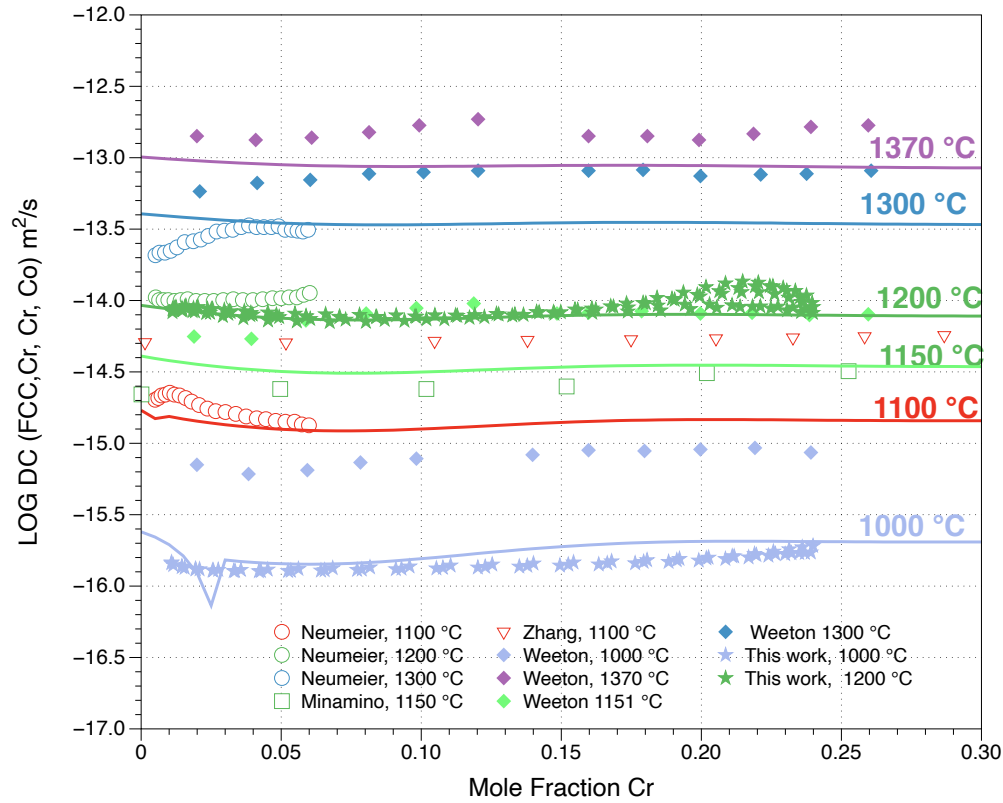


Figure 4. Cr interdiffusion coefficients as a function of composition. Symbols represent experimental measurements from [7], [56], [29], [51] and this work. The solid lines are the predictions using the current assessment.

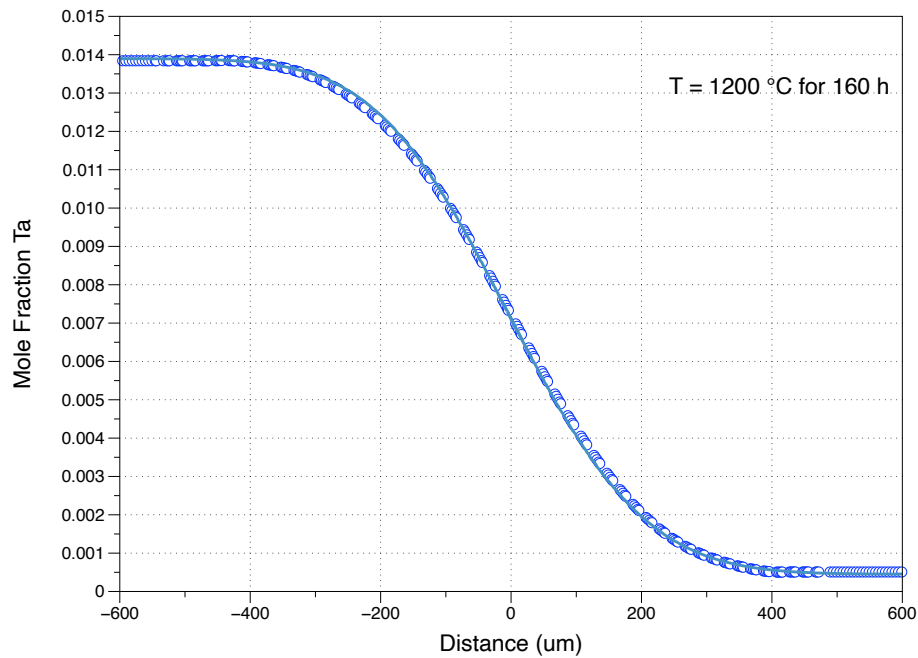


Figure 5. Ta composition profile as a function of distance for the Co/Co-0.014Ta mole fraction diffusion couple after 160 h at 1200 °C. The open symbols represent the measured compositions and the solid line is the predicted composition profile.

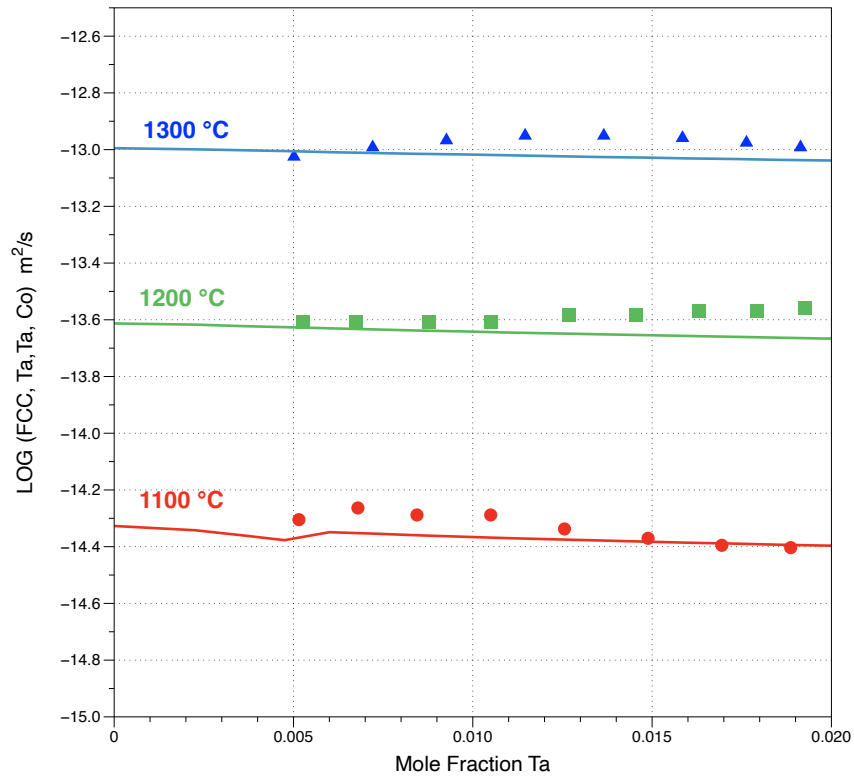


Figure 6. Interdiffusion coefficients as a function of Ta concentration. Symbols are the data from Neumeier [7]. The solid lines are the current assessment.

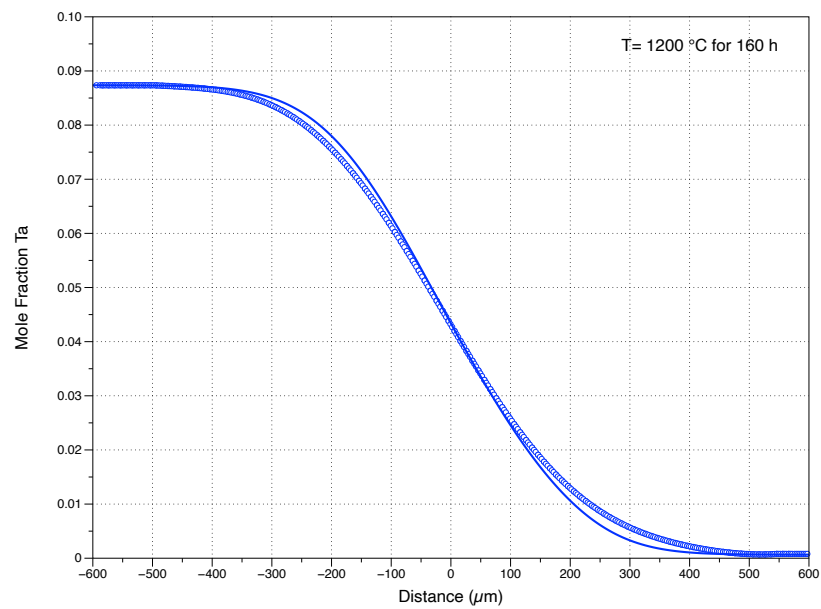


Figure 7. Mole fraction Ta as a function of distance for the Ni/Ni-0.087 Ta mole fraction diffusion couple after 160 h at 1200 °C. Symbols are the experimental data. Solid line is the current assessment.

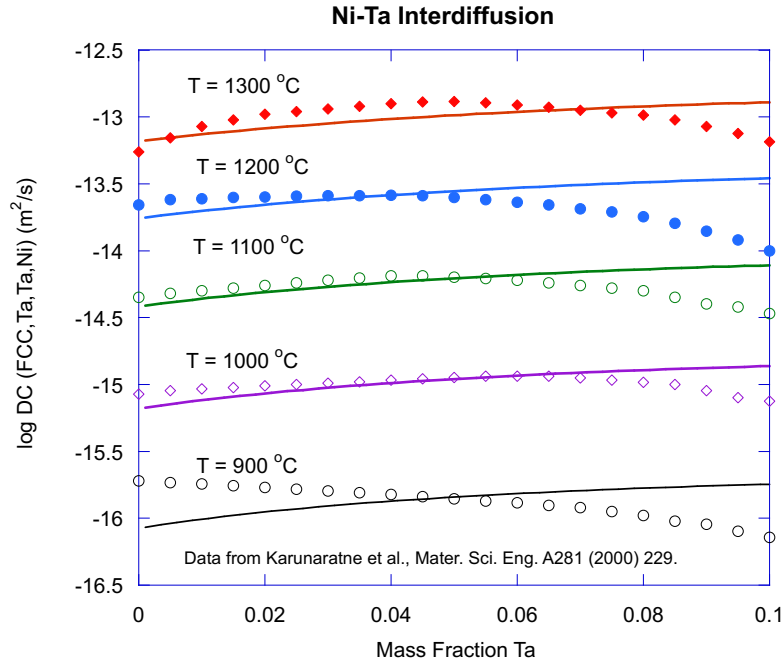


Figure 8. Measured and predicted interdiffusion coefficients of Ta in Ni as a function of Ta. The open symbols are the experimental measurements from Karunaratne et al. [38] and the solid lines are the predicted interdiffusion coefficients.

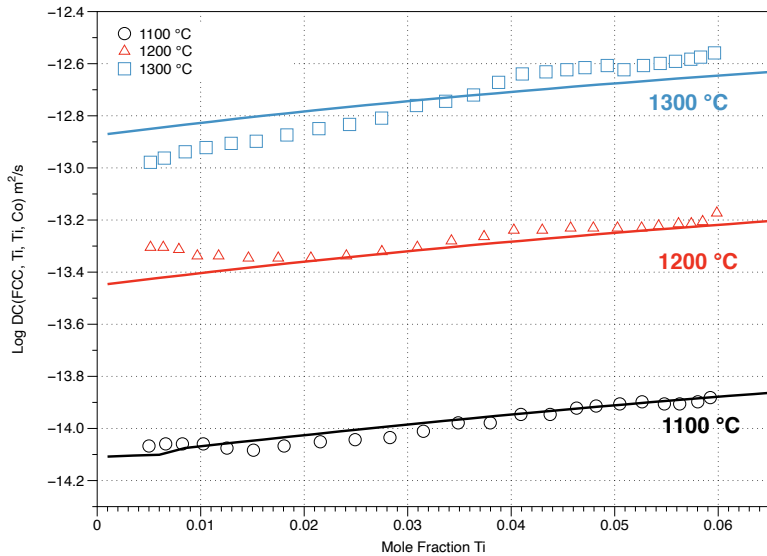


Figure 9. Interdiffusion coefficient of Ti in Co as a function of mole fraction Ti at 1100 °C, 1200 °C and 1300 °C. The open symbols are experimental measurements by Neumeier [7] and the solid lines are the predicted interdiffusion coefficients.

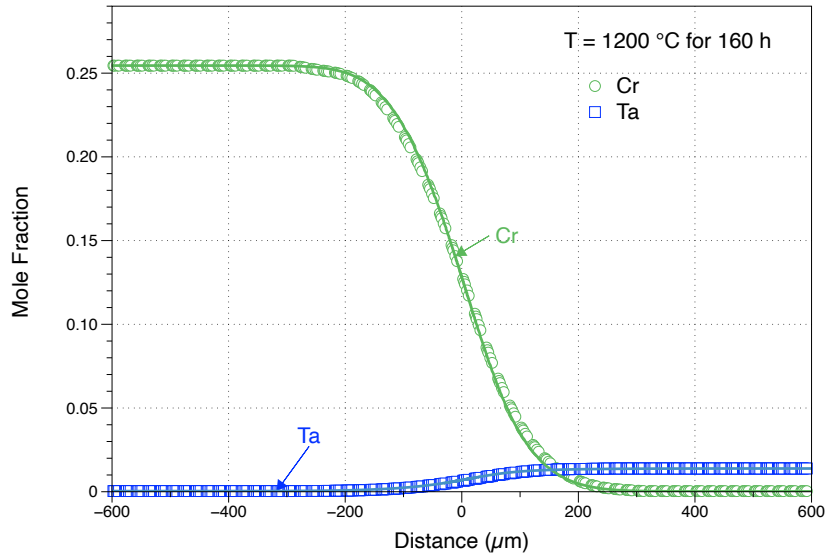


Figure 10. Measured (open symbols) and predicted (solid lines) composition profiles for the Co-0.25 Cr mole fraction/Co-0.014 Ta mole fraction diffusion couple at 1200 °C for 160 h.

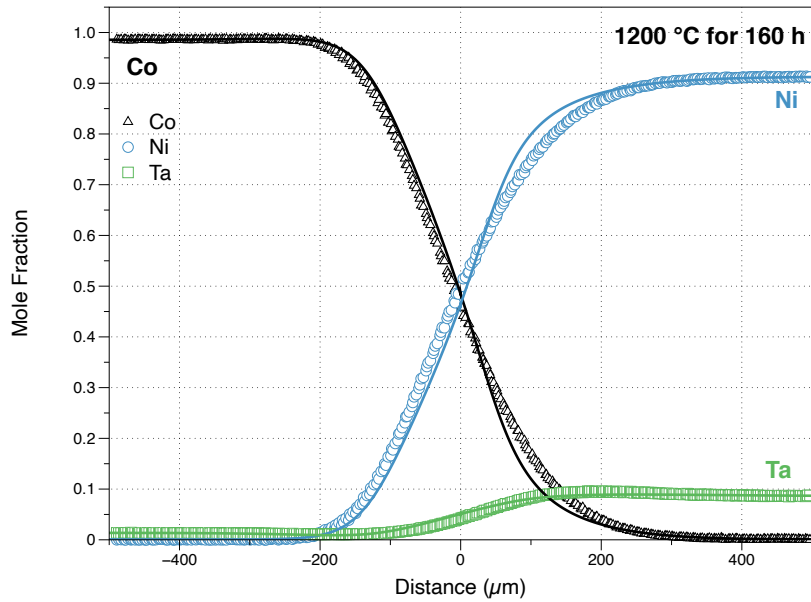


Figure 11. Measured (open symbols) and predicted (solid lines) composition profiles for the Co/Ni-0.10 Ta mole fraction diffusion couple at 1200 °C for 160 h.

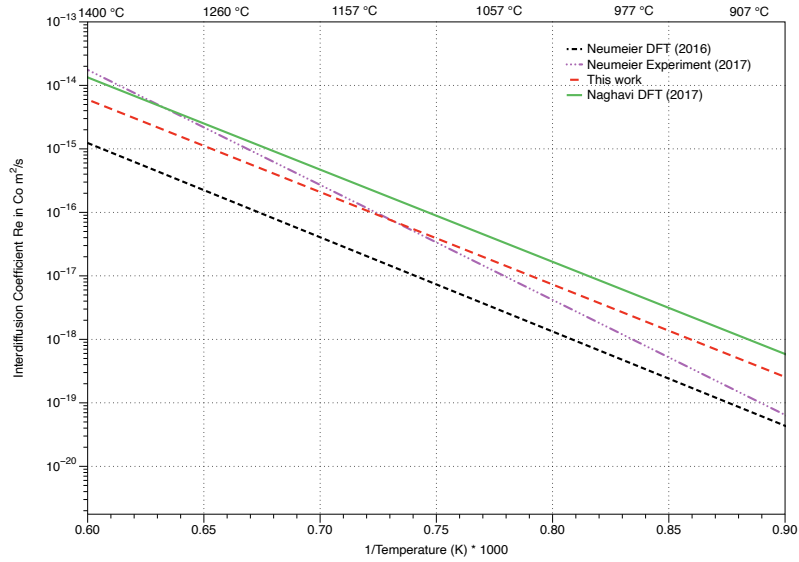


Figure 12. Interdiffusion Coefficient of Re in Co as a function of temperature comparing results from [6], [7] and the current assessment.

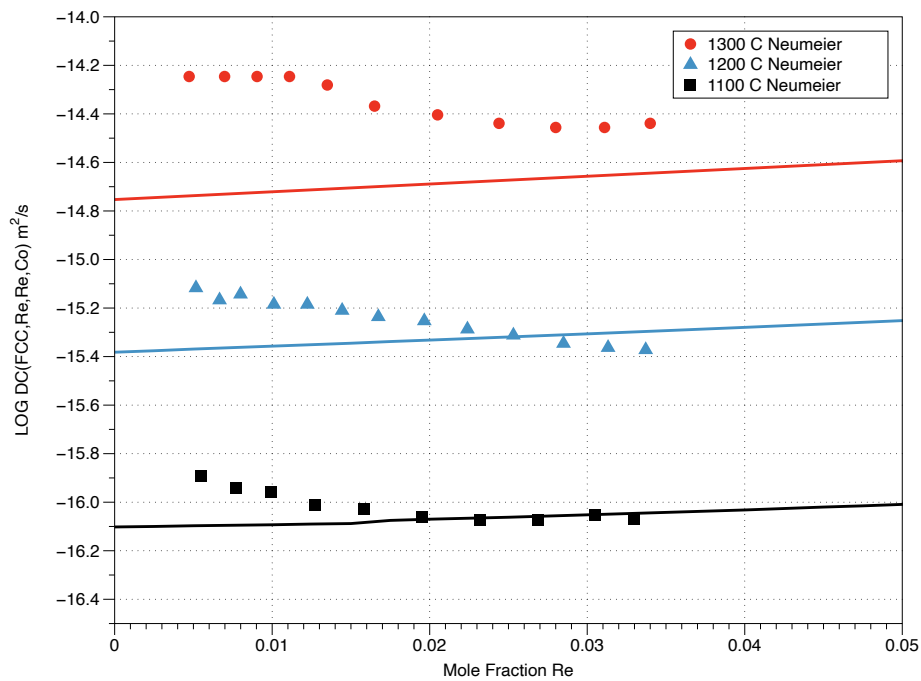


Figure 13. Interdiffusion Coefficient of Re in Co as function of the mole fraction Re. Solid symbols represents the experimental data from Neumeier [7] and the solid lines are the predicted interdiffusion coefficient.

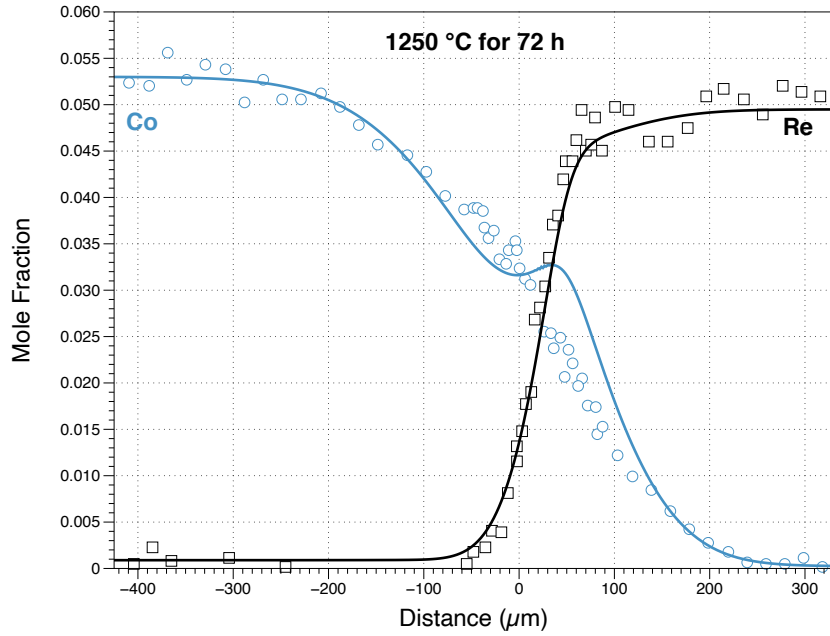


Figure 14. Composition profiles for the Ni-0.05 mole fraction Co / Ni-0.05 mole fraction Re diffusion couple for 1250 °C for 72 h. The open symbols are the experimental measurements [53] and the solid lines the simulation results.

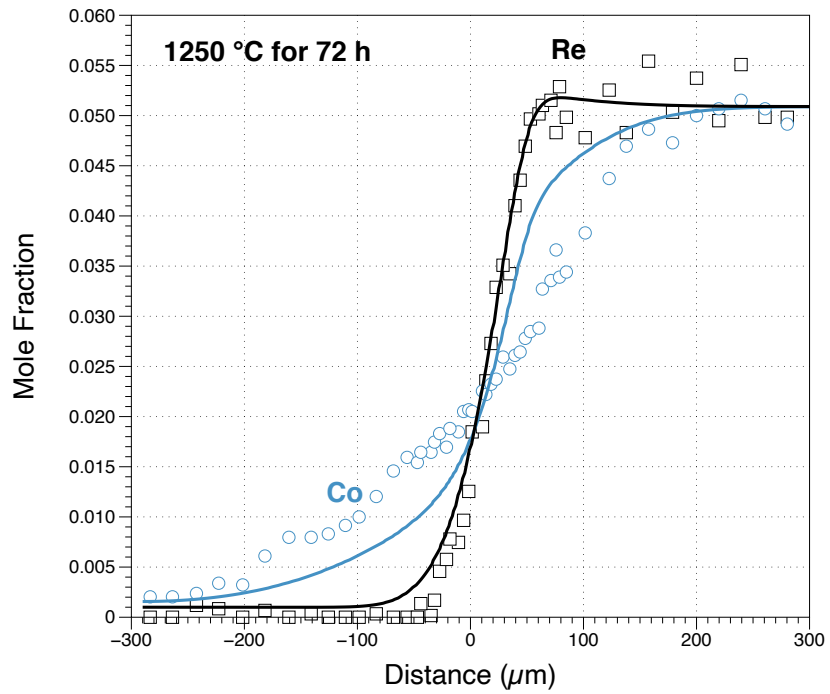


Figure 15. Composition profiles from the Ni/Ni-0.05 Co-0.05 Re mole fraction at 1250 °C for 72 h. The open symbols represent the experimental data from [53] and the solid lines are the simulation predictions.

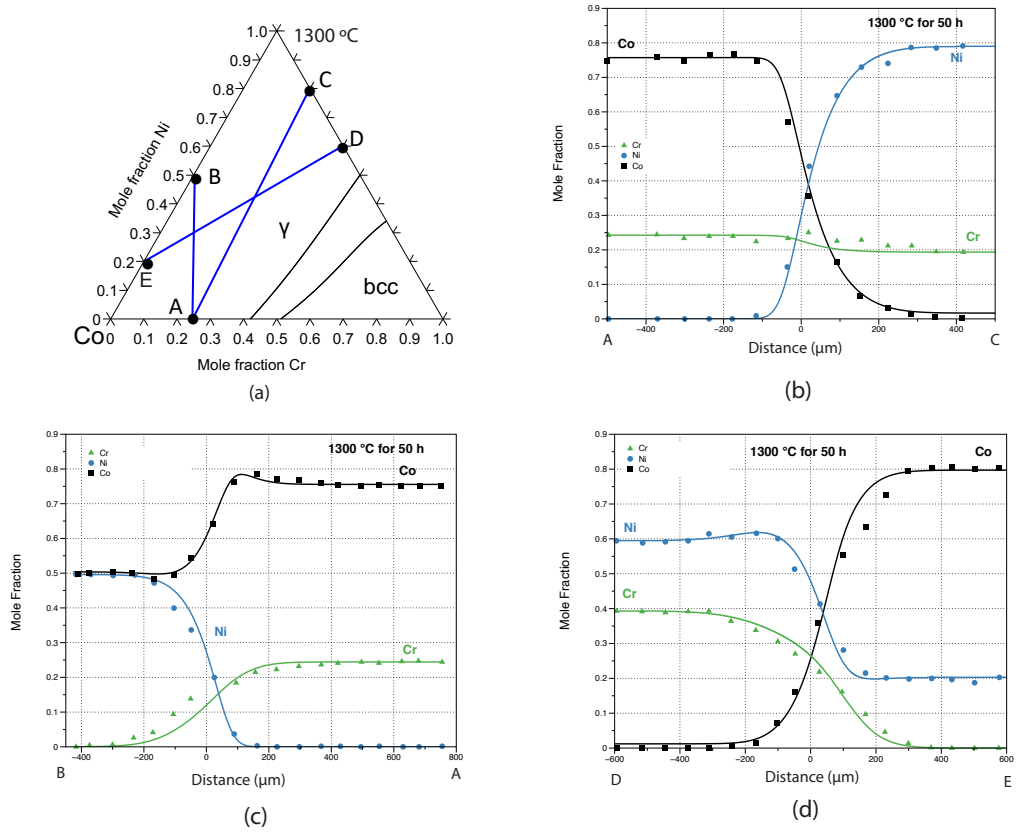


Figure 16. Interdiffusion couples in the Co-Ni-Cr system at 1300 °C as reported by Chen et al. [49] (a) The isothermal Co-Cr-Ni section at 1300 °C showing diffusion couples in the FCC phase region. (b) The A/C diffusion couple composition profiles. (c) The B/C composition profiles and (d) the D/E composition profiles. The symbols are the experimental data and the solid lines are the simulation predictions.

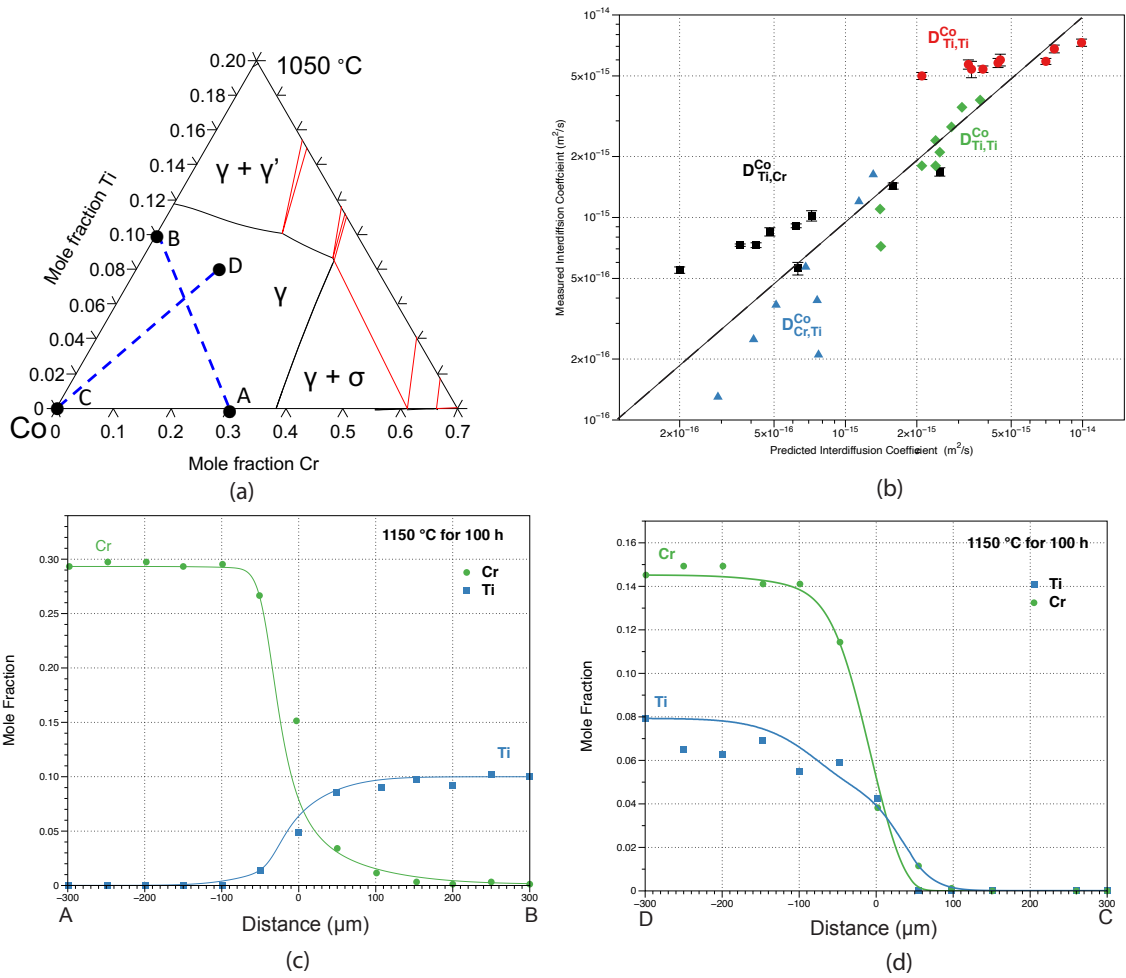
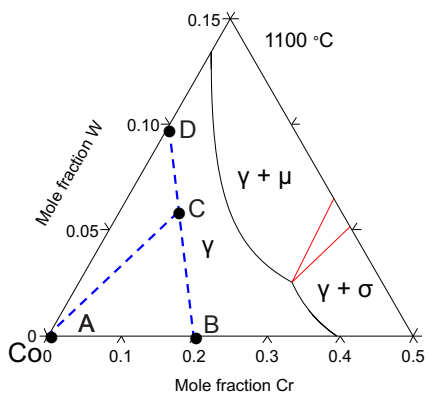
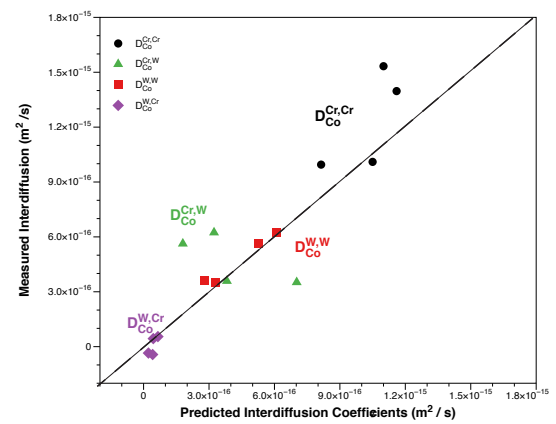


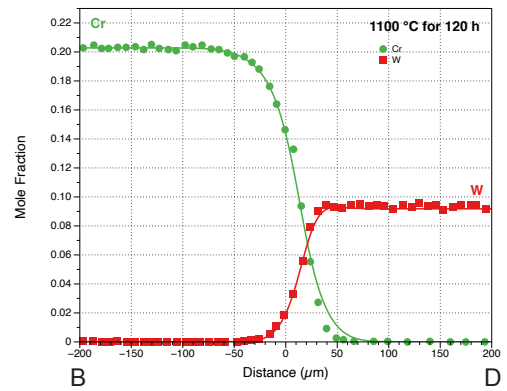
Figure 17. Summary of comparison with Co-Cr-Ti diffusion couples measured Zhou et al. [50] (a) Co-rich isothermal section at 1050 °C indicating the diffusion couple end member locations in the single γ region. (b) Comparison of measured and calculated interdiffusion coefficients at 1050 °C. (c) Measured and predicted Co-0.3Cr/Co-0.1Ti (A/B) mole fraction composition profiles at 100 h at 1050 °C (d) Measured and predicted Co-0.14Cr-0.08Ti/Co-0.1Ti mole (D/E) fraction composition profiles at 100 h at 1050 °C.



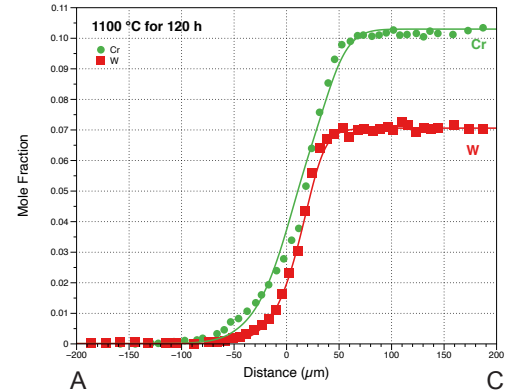
(a)



(b)



(c)



(d)

Figure 18. Summary of diffusivities in the Co-Cr-W system at 1100 °C. (a) Co-rich isothermal section at 1100 C showing the location of the AC and BD diffusion couple end members in the single phase γ region as report by Zhang et al. [51]. (b) Comparison of the measured interdiffusion coefficients [51] and the predicted coefficients. (c) Comparison of the measured and predicted composition profiles for the BD diffusion couple at 1100 °C for 120 h. (d) Comparison of the measured and predicted composition profiles for the AC diffusion couple at 1100 °C for 120 h. For (c) and (d) the experimental work by [51] is represented by the solid symbols and the predictions by the solid lines.

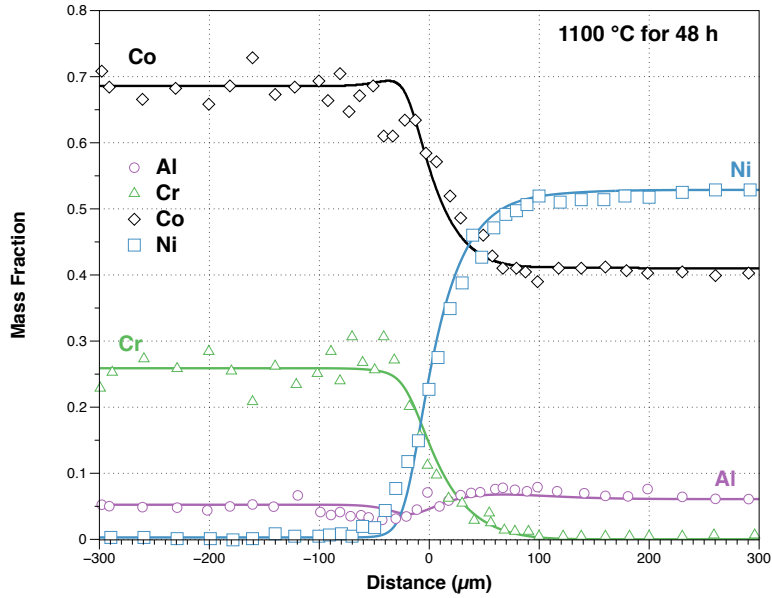


Figure 19. Comparison of the measured and predicted composition profiles for the Co-0.06Al-0.279Cr/ Ni-0.053Al-0.348Co mass fraction at 1100 °C for 48 h. The experimental profiles from Gomez et. al [57] are represented by the open symbols and the current predict composition profiles are represented by the solid lines.

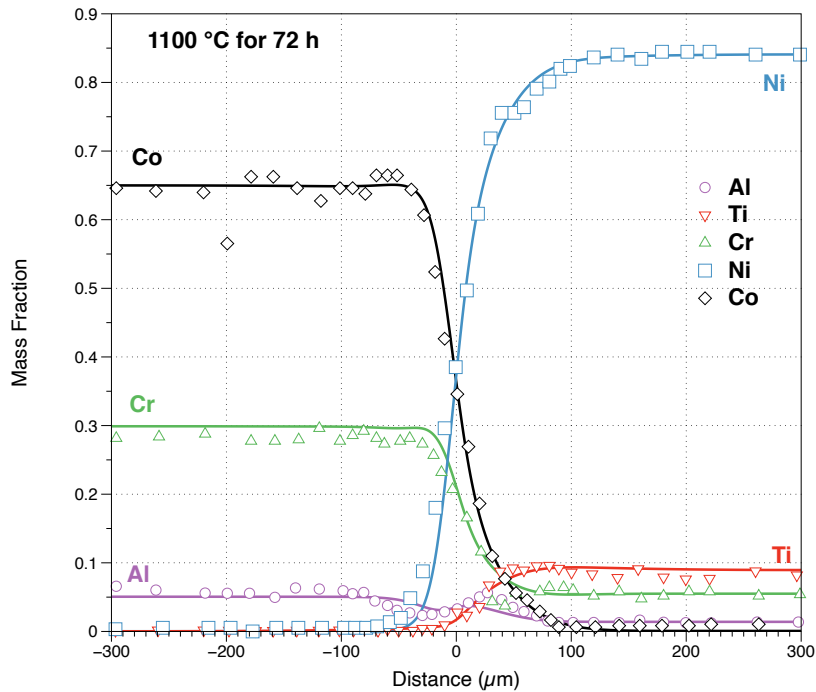


Figure 20. Comparison of the measured and predicted composition profiles for the Co-0.066Al-0.287Cr/ Ni-0.014Al-0.055Cr-0.089Ti mass fraction at 1100 °C for 72 h. The experimental profiles from Gomez et. al [57] are represented by the open symbols and the current predict composition profiles